LASER & PHOTONICS REVIEWS
www.lpr-journal.org

Recent Advances in the Functionalization of Perovskite Solar Cells/Photodetectors

Diandian Wang, Wenjie Cheng, Chao Wang, Min Zhou, Wei Tian, and Liang Li**

Metal halide perovskite materials have excellent photoelectric properties, including high absorption coefficient, long charge carrier diffusion length, and low exciton binding energy, making them excellent candidates for photoconversion devices. In the past decade, great progress has been made in improving the performance of perovskite-based solar cells and photodetectors. However, perovskite devices need to be endowed with more functionality to meet practical application requirements. In this regard, the three major trends in perovskite device development involving flexibility, transparency, and self-healing have attracted wide interests. This review first summarizes the fundamental design principles of endowing perovskite devices with more functionality. Specifically, the functionalization is realized through elaborate substrate and electrode selection, perovskite layer modification, and device layout. This review presents the recent advances and specific requirements for functionalization of perovskite devices according to the three basic components: substrate, electrode, and perovskite layer. Finally, potential challenges and future research directions in this field are outlined. The aim of this review is not only to shed light on the basic design principles of functionalized perovskite devices, but also to serve as the roadmap for future exploration in perovskite devices.

1. Introduction

Organic–inorganic metal halide perovskite materials have excellent photoelectric properties, such as high absorption coefficient, long charge carrier diffusion length, and low exciton binding energy, making them excellent candidates for optoelectronics devices.[1–6] With recent research advances in additive engineering, interface modification, and device layout, the performance of perovskite photodetectors (PPDs) and perovskite solar cells (PSCs) has been developed to a high level. So far, the world's highest efficiency of single junction PSCs has reached 25.6%. The optical responsivity (R) of highly-efficient PPDs has exceeded 10^9 A W^{-1} and the specific detection rate (D^*) has exceeded 10^{16} Jones.[7–9] Unfortunately, the rigid, opaque, and instable characteristics of perovskite devices impede the commercial development of PPDs and PSCs in the long run when exposed to external forces, continuous illumination, moisture, and high temperature or used as a smart photovoltaic window. Thus, empowering perovskite optoelectronics devices with particular capabilities has become a promising way to efficaciously improve the device application scope and long-term durability.[10–14] Recently, the functionalization of PPDs and PSCs has become a significant development direction. Flexible and stretchable perovskite devices have potential application prospects in areas such as cheap portable and wearable photovoltaics.[15,16] Semitransparent solar cells and photodetectors can be used as windows in buildings and skyscrapers to provide shading and green electricity for buildings and can form a series circuit with other mature solar cells to achieve higher efficiency.[17,18] A perovskite photovoltaic device with self-healing refers to one that can, after the device decomposes under the influence of the external environment or breaks due to bending and stretching, resume its original state and continue to work, which greatly improves the service lifespan of the device.[19,20] In short, flexible, semitransparent, and self-healing devices have broad application prospects. More importantly, in the preparation of these three functionalized optoelectronic devices, the researchers found that flexibility, semitransparency, and self-healing are compatible. In recent years, great progress has been made in this field. Due to the increasingly large number of investigations that have been performed, a comprehensive and timely review of the functionalization of PPDs/PSCs is necessary to summarize the great advances in this field. Nevertheless, no in-depth reviews on the design strategies and material exploration in the functionalization of PPDs/PSCs are found in literature to date.

Herein, we present a review on design strategies of functional perovskite devices according to the substrate and electrode selection, material engineering, and device configurations. The first part elaborates on the main strategies for realization of the flexibility of perovskite devices according to different substrates,

D. Wang, W. Cheng, C. Wang, W. Tian, L. Li
School of Physical Science and Technology
Center for Energy Conversion Materials & Physics
Jiangsu Key Laboratory of Thin Films
Soochow University
Suzhou 215006, P. R. China
E-mail: wtian@suda.edu.cn; lli@suda.edu.cn
M. Zhou
College of Physical Science and Technology
Yangzhou University
Yangzhou 225002, P. R. China

The ORCID identification number(s) for the author(s) of this article can be found under https://doi.org/10.1002/lpor.202200641

DOI: 10.1002/lpor.202200641

 © 2022 Wiley-VCH GmbH

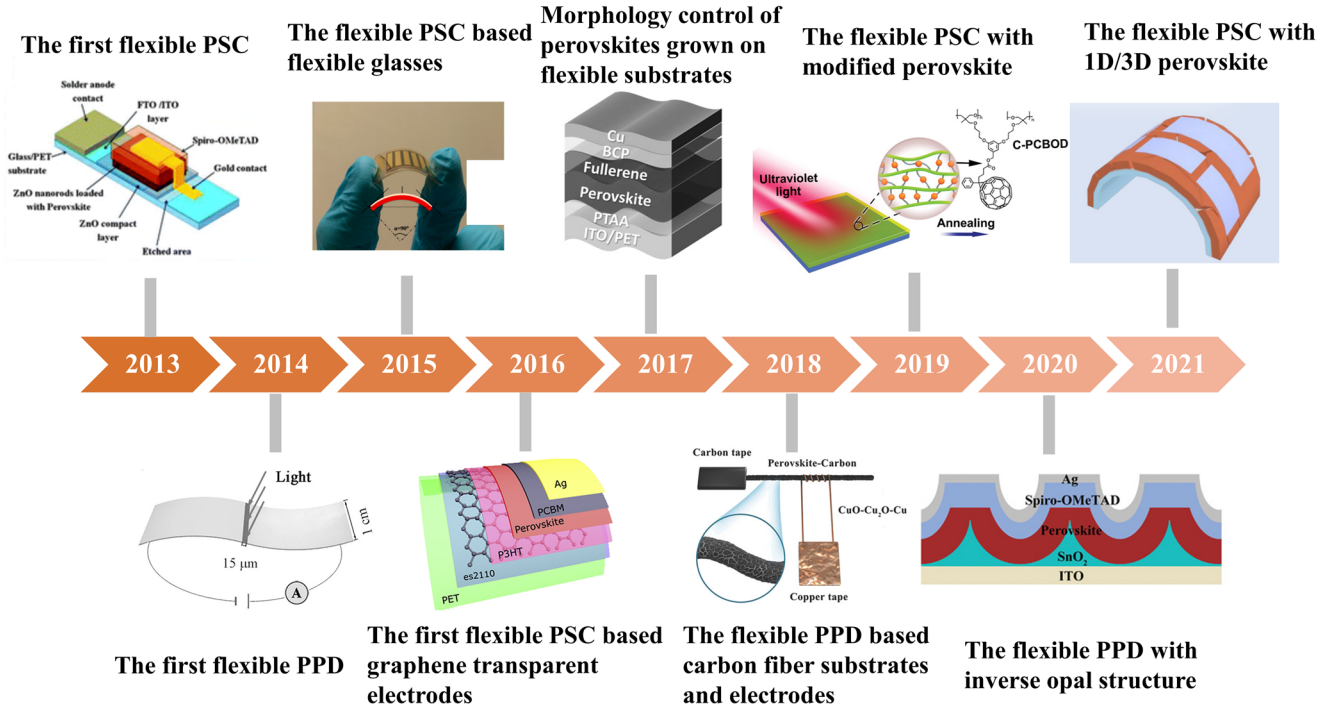


Figure 1. A timeline of representative works on flexible PSCs and PPDs. The first flexible PSC. Reproduced with permission.[3] Copyright 2013, The Royal Society of Chemistry; The first flexible PPD. Reproduced with permission.[23] Copyright 2014, Wiley-VCH; The flexible PSC based flexible glasses. Reproduced with permission.[51] Copyright 2015, American Chemical Society; Reproduced with permission.[58] Copyright 2016, Elsevier Ltd; Morphology control of perovskites grown on flexible substrates. Reproduced with permission.[80] Copyright 2017, Wiley-VCH; The flexible PPD based carbon fiber substrates and electrodes. Reproduced with permission.[33] Copyright 2018, Wiley-VCH; The flexible PSC with modified perovskite. Reproduced with permission.[81] Copyright 2019, Wiley-VCH; The flexible PPD with inverse opal structure. Reproduced with permission.[88] Copyright 2020, Wiley-VCH; The flexible PSC with 1D/3D perovskite The flexible PSC with modified perovskite. Reproduced with permission.[87] Copyright 2021, Elsevier Inc.

electrodes, and perovskites. For the second part, we summarize recent progress on semitransparent perovskite devices. Then, the approaches to achieve self-healing function are summarized. Finally, we provide an overall summarization and discussion about the future development directions of functionalization of perovskite devices, as well as the potential challenges.

2. Flexible PSCs and PPDs

Flexible devices have received wide attention due to their broad application in wearable, portable, foldable and deployable devices.[15,16] Whether it is a PSC with a conventional structure or an inverted structure or a photoconductor/phototransistor/photodiode, it consists of at least the following three parts: a substrate, an electrode, and a perovskite layer. Therefore, the flexibility of these three parts is crucial to the mechanical stability of the final device. **Figure 1** depicts a timeline of representative works on flexible perovskite devices, and the focus of these works is mainly on the substrate selection, electrode design, and perovskite layer engineering. The following section mainly discusses the development process of flexible devices from the perspective of these three aspects.

2.1. Flexible Substrate

The substrate is one of the most basic components of a perovskite optoelectronic device, and its flexibility is very important to realize the flexibility of the device. In recent years, polymer substrates such as polyethylene terephthalate (PET), polydimethylsiloxane (PDMS), and polyimide (PI) have been commonly used as flexible substrates.[21–25] These polymers and substrates have the advantages of good flexibility, great stability, and excellent transparency and initially became the researchers' first choice.[15,21,22]

Xie's group was the pioneer in preparing flexible PPDs based on PET/$MAPbI_3$, which showed good light response and flexibility (**Figure 2**a).[23] This PPD exhibited a high light-dark current ratio, swift response speed, outstanding stability, and reproducibility. In addition, after bending several times, the photocurrent change of the PPD under 365 and 780 nm illumination was almost negligible; thus, it showed good flexibility (Figure 2b). Inspired by this work, flexible PPDs based on flexible polymer substrates continue to be developed. As shown in Figure 2c, our group prepared flexible PPDs based on $MAPbI_3$ polycrystalline film on a polyethylene naphthalate (PEN) substrate and achieved a detectivity (D^*) of up to 10^{13} Jones.[24] When the bending angle of the device was increased from 0° to 120°, the photocurrent and response speed remained basically unchanged (Figure 2d). When the bending angle and cycle were as high as 180° and 200 cycles, respectively, the photocurrent only showed a small drop (Figure 2d, e). Recently, Ding et al. deposited perovskite on a PEN substrate treated with a brominated (3-aminopropyl) triethoxysilane self-assembled monolayer (APTES). By simply soaking the substrate, the hydroxyl groups of APTES molecules can easily react with the hydroxyl groups on the surface of silica through a

© 2022 Wiley-VCH GmbH

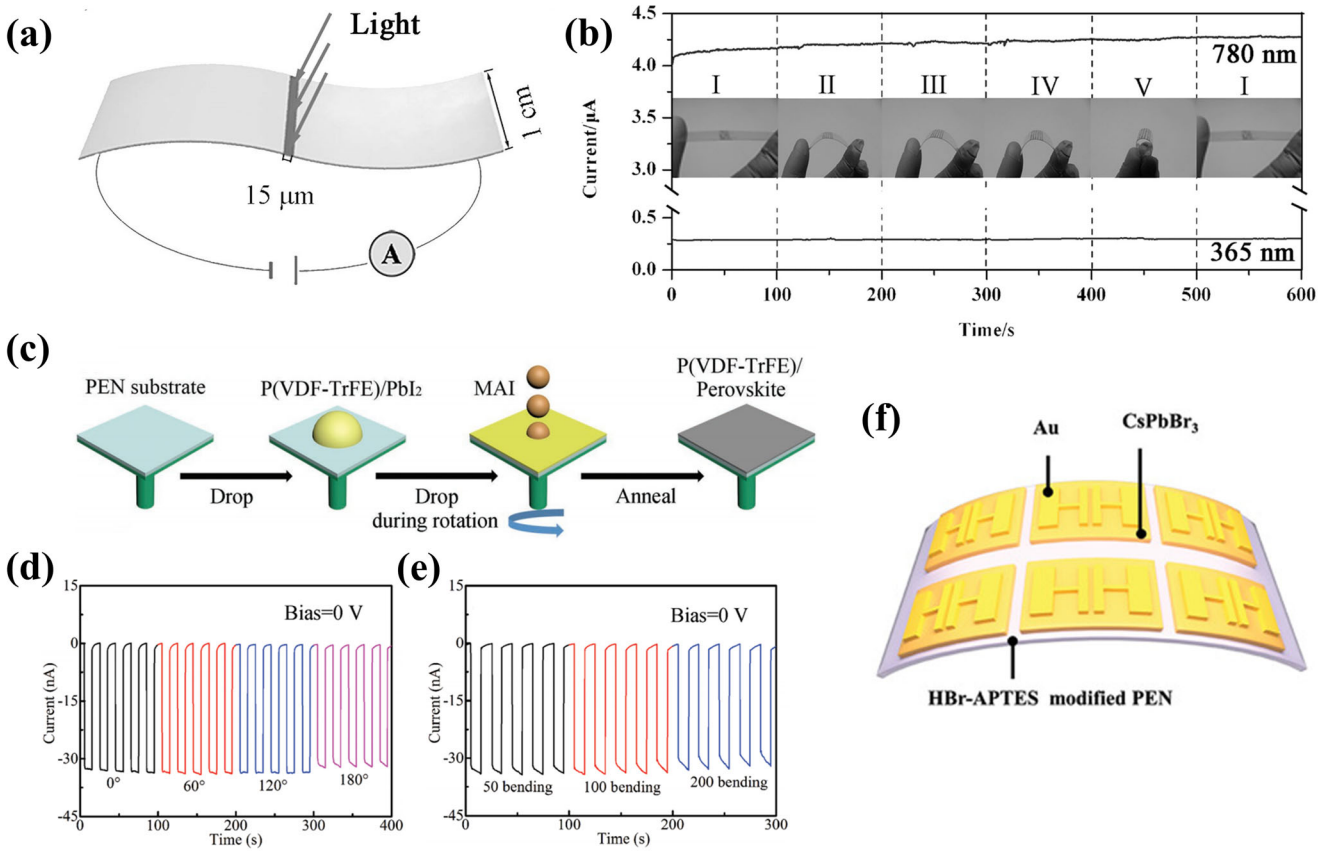


Figure 2. a) Schematic diagram of the $MAPbI_3$ photodetector. b) The *I–t* curves of a flexible hybrid photodetector bent with different curvatures at a bias voltage of 3.0 V, and the light intensities are 365 nm for 0.01 mW cm^{-2} and 780 nm for 0.2 mW cm^{-2}. The inserts are photographs of the device with different bending diameters. Reproduced with permission.[23] Copyright 2014, Wiley-VCH. c) Schematic illustration of the process of fabricating perovskite thin films on PEN substrates. *I–t* curves of the device under white light illumination at d) different bending angles and e) different bending cycles. Reproduced with permission.[24] Copyright 2019, Wiley-VCH. f) Schematic illustration of the flexible photodetector array device based on PEN substrates. Reproduced with permission.[26] Copyright 2021, Wiley-VCH.

condensation reaction. This results in the formation of strong Si—O—Si covalent bonds between the substrate and the APTES layer. Using it as the medium between the perovskite and the substrate can increase the affinity between the perovskite and the substrate, which is conducive to the growth of uniform perovskite films to significantly improve the morphology of the films and obtain larger particles (Figure 2f), thereby improving the photosensitivity of the films and enhancing the mechanical stability of the flexible devices.[26]

Despite great progress on optoelectronic devices based on flexible polymer substrates, it is worth noting that the polymer substrate is expensive, not resistant to high temperature, and has limited flexibility, which limits its wider application.[27–29] Therefore, other flexible substrates have been developed as alternatives to polymer substrates. Carbon cloth has attracted researchers' attention because of its excellent high temperature resistance, strong strength, good electrical conductivity, and high cost-effectiveness.[30,31] On this basis, our group employed carbon cloth as a substrate for the first time to prepare flexible PPDs (**Figure 3**a),[32] which showed a wide spectral response, high responsivity, and fast response speed, and the device still maintained good light response ability under 80 bending cycles and an extreme bending angle of 180° (Figure 3b). This work lays a foundation for the development of low-cost, flexible, and self-powered broadband PPDs. However, the perovskite coverage is uncontrollable due to the interweaving of carbon fibers, which leads to an unsatisfactory *R*. Compared with carbon cloth, the carbon fiber component can be formed into a better shape and integrated with other equipment using weaving technology. Later, our group fabricated devices with a structure consisting of double-twisted perovskite-TiO_2-carbon fiber and CuO-Cu_2O-Cu wire (Figure 3c),[33] where carbon fiber was used as a flexible substrate, and carbon tape was used to protect the carbon fiber; CuO broadened the range of the response spectrum and promoted the extraction of holes; and Cu_2O inhibited charge recombination due to its suitable valence band position. Finally, the device exhibited excellent performance, with a light response range from 350 to 1050 nm and a D^* as high as 10^{13} Jones, and still maintained good light response performance and extremely fast response speed under 60 cycles and 150° bending conditions (Figure 3d). This special and novel device structure has high performance, wide detection range, self-powered capability, and excellent flexibility, which lays the foundation for future wearable electronic devices.

© 2022 Wiley-VCH GmbH

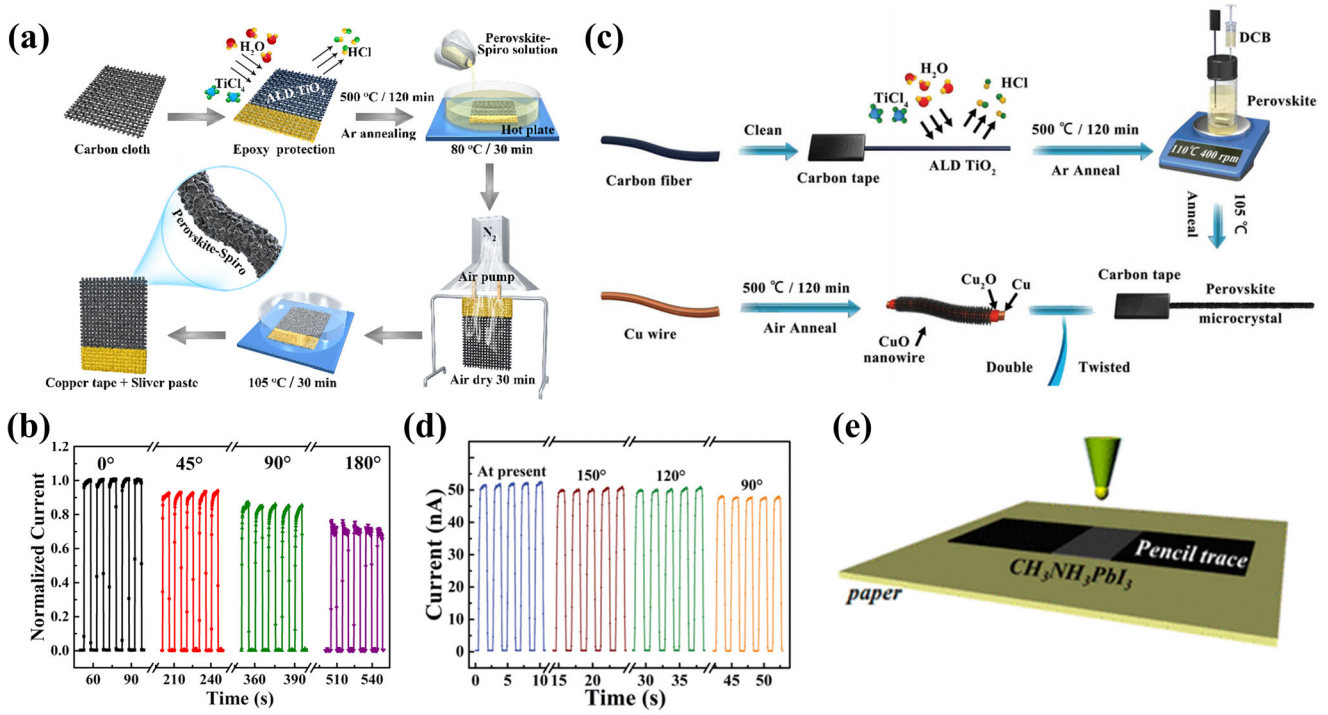


Figure 3. a) Schematic illustration of the process of fabricating a flexible perovskite photodetector on carbon cloth. b) Normalized *I–t* curves at different bending angles. Reproduced with permission.[32] Copyright 2017, Wiley-VCH. c) Schematic illustration of the fabrication process for constructing a fiber-shaped photodetector. d) *I–t* curves under different bending angles at zero bias. Reproduced with permission.[33] Copyright 2018, Wiley-VCH. e) Schematic illustration of fabricating PPD-based $CH_3NH_3PbI_3$ directly on the paper substrate. Reproduced with permission.[39] Copyright 2017, American Chemical Society.

Paper, as a green, nonpolluting, degradable, foldable, and lightweight material, is considered a potential material for flexible electronic products.[34–38] In 2017, Yan's group combined paper and perovskite to prepare a flexible device for the first time and used a pencil to draw a pair of graphite electrodes as an external circuit (Figure 3e).[39] Finally, they obtained an R of 4.4 mA W^{-1} and a response speed of <10 ms. The device maintained good light response performance after 1000 cycles of bending. This group obtained 3D PPDs through origami technology, which can distinguish the direction of the incident light after processing the signal. This unique 3D structure has spatial recognition ability that traditional 2D does not have, which provides a novel idea for the preparation of 3D devices in the future. At present, there is still much research space for optoelectronic devices based on paper substrates.

In addition to the abovementioned materials, mica, flexible glass, and metal foil can also be used as flexible substrates. Mica has good transparency, high heat resistance, excellent mechanical flexibility, abundant reserves, and easy processing characteristics, making it one of the options for flexible substrates.[40–43] Huang's group proved that mica is a very promising candidate substrate for flexible optoelectronics that is worthy of in-depth study.[41] After that, Li's group fabricated PSCs on a transparent layered mica substrate, and the device maintained an efficiency of over 91.7% after being bent for 5000 cycles.[44] Due to the high flexibility of the mica substrate and van der Waals epitaxial growth of transparent conductive indium tin oxide (ITO), the device shows excellent flexibility. These advantages greatly relax the mechanical constraints on PSC and reduce the strain on the device even under large bending deformation. Metal foil has high flexibility, conductivity, and excellent high-temperature resistance and is considered a promising flexible substrate.[45–47] Jun's group used Ti metal as a flexible substrate for the first time, and the prepared PSCs showed very little variation in efficiency after 100 cycles of bending.[48] However, the manufacturing process of PSCs usually requires temperatures as high as 100 °C. The thermal expansion of the metal substrate in this temperature range is still significant, which introduces stress and strain, resulting in lower performance.

The substrate commonly used for rigid devices is glass, which has the advantages of high transparency, high temperature resistance, and chemical stability. When the thickness of the glass is reduced to a certain degree, it will have a certain degree of bending flexibility, so it can be used as a flexible substrate.[49,50] For example, Fan's group controlled the glass thickness to ≈50 microns to obtain flexible glass for the first time.[51] After 200 cycles of bending with a bending diameter of 4 cm, the power conversion efficiency (PCE) of the PSC was reduced from 11.7% to 11.24%. Afterward, Huang's group introduced NH_4Cl into the perovskite precursor solution to prevent the formation of voids between perovskite and glass, and the PCE of the final device was close to 16%.[52] More importantly, this ultrathin glass and solution coating strategy is helpful for the realization of high-throughput and high-speed manufacturing.

In short, flexible substrates are important parts of flexible devices. In this section, we discuss some flexible substrate

© 2022 Wiley-VCH GmbH

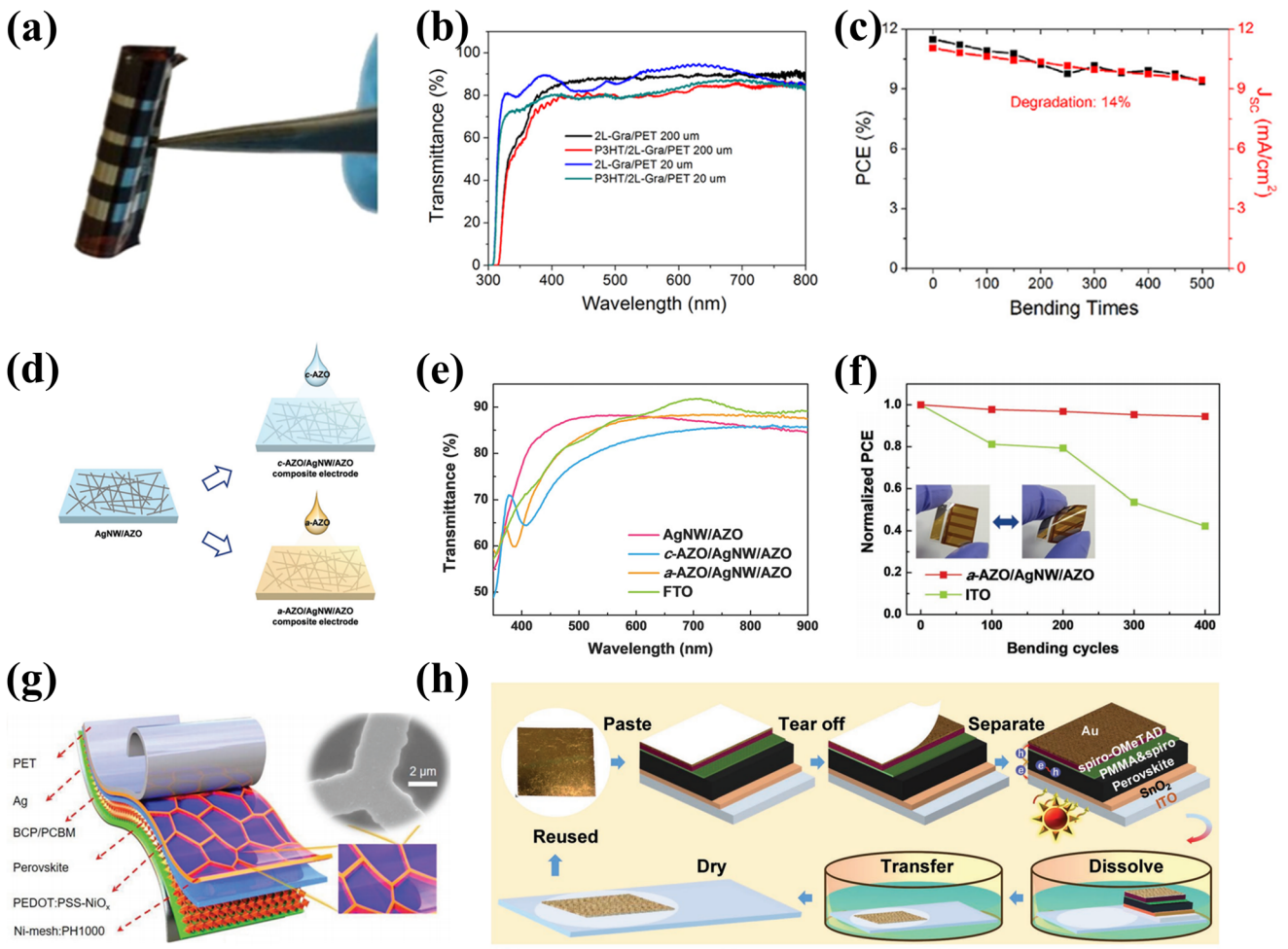


Figure 4. a) Photograph of flexible PSC based graphene as a transparent electrode. b) The transmittance of PET substrates (thickness: 20 or 200 mm) coated with 2-layer CVD graphene and P3HT layers. c) PCE and J_{SC} of the PSC as functions of the bending radius. Reproduced with permission.[58] Copyright 2016, Elsevier Ltd. d) Schematic of the c-AZO/AgNW/AZO and a-AZO/AgNW/AZO composite electrodes. e) Transmission spectra of AgNW/AZO and AZO/AgNW/AZO composite electrodes and an FTO electrode. f) Mechanical bending test results of PSCs on ITO/PEN and a-AZO/AgNW/AZO/PES electrodes. The insets are the photographs of the device before and after bending. Reproduced with permission.[67] Copyright 2018, Wiley. g) Schematic illustration of the PET/Ni-mesh substrate. Reproduced with permission.[69] Copyright 2020, Wiley-VCH. h) Schematic of the fabrication and restoration process of the nanoporous Au electrode in PSCs. Reproduced with permission.[70] Copyright 2020, Wiley-VCH.

materials, among which flexibility and transparency are their most basic characteristics. During process of the manufacturing these devices, a suitable substrate can be selected according to the actual needs.

2.2. Flexible Electrode

Flexible electrodes play a significant role in flexible devices because the electrodes are the bridge connecting the various components of the device. The ideal flexible electrode should have good mechanical flexibility, bending durability, high conductivity, and high transparency.[53,54] Commonly used flexible transparent electrodes are ITO, poly(3,4-ethylenedioxythiophene):poly(styrenesulfonate) (PEDOT:PSS), aluminum-doped zinc oxide (AZO)/Ag/Au, etc. However, ITO easily becomes brittle; PEDOT:PSS is prone to absorb moisture, which causes the decomposition of perovskite, which negatively affects the long-term stability of the device. Ag and Au need to be prepared in a vacuum and are expensive, which limits the further development of flexible devices; and metal electrodes, especially Ag, are prone to diffuse, which will destroy the perovskite layer. Therefore, it is a need to develop other flexible electrodes.

Graphene has excellent light transmittance over a wide wavelength range, high carrier mobility, good chemical stability, and good mechanical flexibility,[55–57] so it can be used as a material of choice for flexible electrodes. In 2016, Yan's group used graphene as a transparent electrode for flexible PSCs for the first time (**Figure 4**a).[58] This graphene has good transmittance (Figure 4b). The flexible PSCs based on graphene electrodes maintained 86% PCE under bending test conditions for 500 cycles at a bending diameter of 0.175 cm (Figure 4c). It was found that the decrease in the PCE was mainly due to the decrease in the short-circuit current caused by the fracture of the perovskite layer and the top

© 2022 Wiley-VCH GmbH

electrode Ag after the bending test, while the graphene electrode morphology changed little. Afterward, Guo's group prepared all-carbon electrode flexible PSCs,[59] in which graphene and CNTs were used as the front transparent electrode and the back electrode, respectively. The all-carbon electrode-based PSC was bent for 200 cycles with the bending diameter range from 8–2.2 mm. The PCE maintained ≈85% of the original value. After 2000 bending cycles, the PCE maintained 80% of the original efficiency. Compared with devices with ITO/Ag as the electrodes, the flexibility was greatly increased. Moreover, the performance degradation of all-carbon electrode flexible devices may be mainly due to the fragility of the perovskite layer and the delamination of the device.

Metal nanowires (NWs), due to their low sheet resistance, high transmittance, and solution handling properties, are used as alternative conductive transparent electrodes in various optoelectronic devices.[59–62] Due to the good ductility of Ag metal, Ag NWs have good flexibility, making them suitable for the preparation of flexible devices. However, Ag NWs have the following two shortcomings: one is that they are prone to poor contact with the substrate, leading to electrical conductivity and thermal instability,[63,64] and the other is that Ag easily reacts with halogen elements in the perovskite,[65,66] resulting in poor device performance. Some researchers focus on solving the above problems, but the results show that performance and cost cannot be balanced. Moon's group deposited a layer of nonporous aluminum-doped zinc oxide on Ag NWs (Figure 4d).[67] On the one hand, it protects the chemical stability of the Ag nanowire network (NWN). On the other hand, it solves the problems of poor conductivity and thermal instability caused by weak adhesion to the substrate. Figure 4e shows that the average visible light transmittance of Ag NW/AZO, which was in the range of 400–800 nm (86.7% for AVT/AZO and 85.9% for FTO), comparable to that of commercial FTO electrodes, which indicated that this layer of material has little effect on the light absorption of the perovskite layer. The test results showed that the PCE of the flexible device reached 11.23%, and the device performance was 94% of the initial value after 400 bending cycles at a bending diameter of 12.5 mm (Figure 4f). A method commonly used involves inserting a transparent oxide, such as ITO or metal-doped zinc oxide, between the metal transparent electrode and the perovskite layer as a protective layer, but the mechanical stability of the device is limited by the flexibility of the metal oxide. Therefore, Park's group used graphene as a protective layer to insert between the electrode Cu grid-embedded polyimide and the perovskite[68] due to the conductivity, impermeability, mechanical stability, and chemical stability of graphene. The final test results showed that the device can maintain 97% and 94% of the initial PCE after 10 000 cycles of bending at bending radii of 5 and 7 mm, respectively. However, the PCE of the device was not ideal. As shown in Figure 4g, Wang's group used Ni mesh as a transparent conductive electrode and achieved the best performance of 17.3%.[69] The efficiency of the final flexible device remained at 76% of the initial value after 2000 bending cycles. Compared with the Ag mesh, it showed better mechanical stability. The metal electrodes mentioned above are difficult to recycle and cannot be reused. Therefore, when the metal contact electrode can be reused, the manufacturing cost and environmental pollution will be greatly reduced. Matsuda's group reported on the use of nanoporous Au as the top electrode, where nanoporous gold can be reused, which greatly reduced the cost of manufacturing the device (Figure 4h).[70] The flexible PSCs based on nanoporous Au film maintained 98.5% of the bending durability after 1000 bending cycles, which was higher than the usual flexible PSCs based on evaporated Au. This was because the nanopore structure hindered the generation and propagation of cracks in the nanoporous gold film.

Traditional semitransparent metal oxide electrodes are usually prepared by high-temperature sputtering. Atomic layer deposition (ALD) is another alternative method that has the unique advantages of controllable atomic layer thickness and dense film. Mai's group used ALD to prepare metal oxide electrodes.[71] After the device was bent for 3000 cycles, the light and dark currents did not change significantly.

2.3. Perovskite

Perovskite is a light absorbing material in perovskite optoelectronic devices that has a significant effect on the performance of the material. According to the structure of perovskite, it can be simply divided into the following three types: single crystal, polycrystalline film, and low-dimensional nanostructure perovskites. This section mainly introduces the related exploration in perovskite layers in flexible devices.

2.3.1. Single Crystal

Single crystal perovskites have excellent photoelectric properties, such as a high absorption coefficient, long carrier lifetime, large carrier mobility, low defect state density, and high defect tolerance.[72–76] However, single crystals generally exist in the form of blocks and wafers, which are not suitable for making complex flexible electronic devices and wearable devices, especially because of their fragility. Attracted by the excellent photoelectric properties of single crystal perovskites, researchers have made some attempts in this field, but the initial results are not ideal. One of the challenges of growing single crystal perovskites is that it is difficult to control the growth thickness due to the inherent nature of single crystal growth in all directions. Liu's group successfully prepared a large-area 2D $(PEA)_2PbI_4$ single crystal with a thickness of 0.6 microns through the induced peripheral crystallization method.[77] It should be noted that here 2D perovskite denotes layered 2D Ruddlesden–Popper perovskite (2D represents the crystal structure rather than the micro dimension). The low-dimensional nanostructured perovskites, such as 1D nanowires and 2D nanosheets, will be introduced in Section 2.3.3. PPDs based on ultrathin $(PEA)_2PbI_4$ single crystals exhibited excellent optical and electrical properties, with an external quantum efficiency (EQE) of 26 530%, an R of 98.17 A W^{-1}, and a D^* of 1.62×10^{15} Jones. In addition, it was discovered that during the preparation process, the thickness of the single crystal can be controlled by controlling the cooling rate, and its thickness determined its maximum bending angle, that is, its mechanical flexibility. This work has opened up a path for the application of flexible perovskite single chip microcomputers in high-performance flexible planar light sensors. The successful preparation of flexible 2D layered single crystal materials and devices provides a new material system.

© 2022 Wiley-VCH GmbH

The space-confined method is another simple method for growing single crystal perovskites with controllable thickness, and this method has universal applicability. Wang's group prepared a $MAPbBr_3$ single crystal film by the "space-confined method" and finally reduced the thickness of the single crystal film to 20 nm.[78] The experimental results showed that under the same bending conditions, when the thickness of the single crystal was 20 nm, the photocurrent of the device was basically unchanged, and when the thickness of the single crystal was increased to 809 nm, the photocurrent dropped sharply. The results indicated that as the thickness of the single-crystal increased, the mechanical flexibility of the single-crystal PPDs decreased. Therefore, the best device flexibility was achieved when the thickness was controlled at 20 nm. In addition, the test results showed that the device also had excellent performance with $R = 5600$ and a 3 dB bandwidth of 0.2 MHz. The above results indicated that the thickness of the single crystal was inversely proportional to the mechanical flexibility of the device. Reducing the thickness of the single crystal is a good way to control the flexibility of the device. In addition to 3D perovskite single crystal materials, the space-confined method can also be used to grow 2D perovskite single crystal materials. Recently, Hao's group prepared $EA_4Pb_3Br_{10}$ single crystals with a thickness of ≈220 nm using spatially confined growth.[79] Due to the ferroelectric properties of $EA_4Pb_3Br_{10}$, PPDs based on $EA_4Pb_3Br_{10}$ single crystals have strain modulation ability induced by the piezoelectric photon effect. Under external tensile strain, the response rate can be increased from 0.433 A W^{-1} to 1.233 A W^{-1}, which shows a linear perception of the applied strain. These results greatly enrich the functions of 2D perovskite ferroelectrics and provide a new path for new ferroelectric/piezoelectric devices. In summary, the prerequisite for using single crystal perovskites to make flexible devices is that the single crystal is thin enough to have a certain degree of mechanical flexibility.

2.3.2. Polycrystalline Perovskite Film

Polycrystalline perovskite film can be prepared by a solution spin coating method, which is simple to prepare and inexpensive. In general, devices based on flexible substrates perform slightly worse than devices based on rigid substrates. This is mainly due to the poor quality of the perovskite film grown on the rough surface of the flexible substrate.[80] Therefore, some methods, such as component engineering, additive engineering, and vapor-assisted deposition, are used to enhance the quality of perovskite films. For example, Huang's group obtained a perovskite film grown on a flexible PEI/ITO substrate by adjusting the composition of the perovskite precursor solution,[80] and its morphology and electrical properties were similar to those grown on rigid ITO. They adjusted the ratio of FAI and MABr and increased the short-circuit current and fill factor. In addition, they have greatly increased the size of the crystal grains by DMSO annealing to reduce the density of defect states. The final result showed that the PCE of PSCs based on a flexible ITO/PET substrate increased to 18.1%. Moreover, the PCE of the device dropped to 88.6% of the original value after a bending radius of 4.4 mm was applied, and the device performance still maintained 85.6% of the original value after a bending radius of 4.4 mm was applied for 1000 bending cycles. The test results showed that the decrease in device performance was mainly from the continuous decrease in the fill factor, and the series resistance of the device had increased from 5.4 to 58.8 Ω cm^{-1}, which was probably due to cracks in the flexible ITO after bending.

In addition, the additive strategy can effectively improve the mechanical stability of devices. For example, Abate's group added photocrosslinked [6,6]-phenylC_{61}-butyric oxetane dendron ester (C-PCBOD) to the perovskite layer to improve the quality and mechanical stability of the film.[81] Ultraviolet radiation cross-links the photons in the perovskite film before crystallization occurs, reducing the compressive stress caused by the volume expansion of the perovskite grains. Therefore, the mechanical stability of the device was improved. When the original device was stretched to 10 nm μm^{-1}, the PCE of the device dropped to 42% of the initial value, while the performance of the device based on the C-PCBOD-modified perovskite film maintained 62% of the initial value. Anti-solvent must be used in the one-step spin-coating method to prepare high-quality perovskite films. The application of anti-solvent is extremely sensitive to the processing conditions such as dropping time and amount of solvent, which requires very precise control in fabrication procedures. In addition, most anti-solvents are always toxic and harmful, causing serious pollution to the environment. The anti-solvent method is only suitable for small areas (a few square centimeters, that is, for laboratory-scale equipment), and is difficult to apply to large scale fabrication.[82–84] Liu's group directly added a small amount of MABr into a perovskite precursor to obtain high-quality perovskite thin films without using an antisolvent.[83] The addition of MABr significantly reduces the basic δ-α phase transition energy of FA-based perovskites, and therefore, the annealing temperature of perovskites decreases. Even if the annealing temperature is only 40 °C, the FA-based perovskite can still be transformed into the α phase, and the photoelectric performance is the best when the annealing temperature reaches 100 °C. The reduction of the annealing temperature of FA-based perovskites is a prerequisite for the manufacture of flexible devices. Therefore, the flexible device they prepared achieved a PCE of up to 18.5%, and its performance remained basically unchanged after 1200 bending cycles under environmental conditions.

The above methods mainly improve the flexibility of the perovskite film and the device by improving the quality of the perovskite film. Interface engineering is another effective way to improve the mechanical stability of devices. Interface strain is an inevitable problem in the process of perovskite lattice deformation and crystallization. The accumulation of strain leads to poor material stability, which limits the application of the material in flexible devices. Wang's group introduced organosilane with the molecular formula [$(OC_2H_5)_3$-Si-$(CH_2)_3$-NH_3Br)] (PASCA-Br) as the interface connection material.[85] On the one hand, the two ends of the PASCA-Br molecule can be connected to TiO_2 and perovskite. On the other hand, NH_3Br is also directly used as the structural component of the perovskite crystal lattice unit to release lattice stress on the perovskite side, suppress interfacial tension, and enhance the stability of the device (**Figure 5**a). The test results showed that the device with PASCA-Br had better mechanical stability. After the device was bent 60°, the device performance was still 98% of the initial value (Figure 5b). Chen's group was inspired by human vertebrae and used a

© 2022 Wiley-VCH GmbH

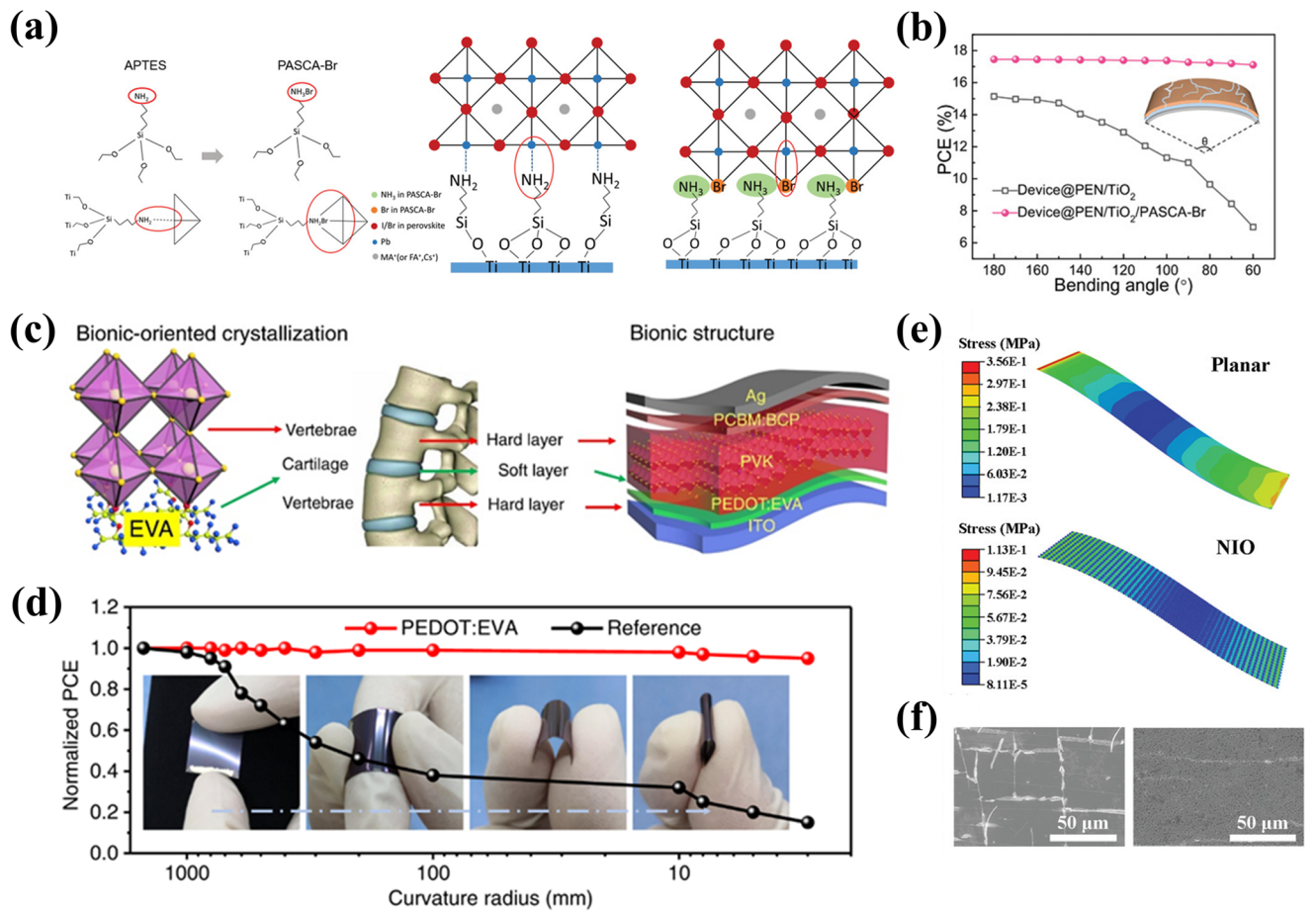


Figure 5. a) Protonated amino terminals (R-NH_3Br) and lattice structure of APTES- and PASCA-Br-modified interfaces. b) PCE changes with different bending angles. The inset is the definition of the bending angle. Reproduced with permission.[85] Copyright 2020, Wiley-VCH. c) Biomimetic mechanisms of the vertebrae and PSCs. d) Normalized averaged PCE values of PSCs after the bending test. The insets are the corresponding photographs of the device under the four bending conditions. Reproduced with permission.[86] Copyright 2020, Nature. e) Finite element simulation of the stress distribution in the planar (up) and NIO (down) perovskite films. f) SEM images of the planar (left) and NIO (right) perovskite films after 200 bending cycles. Reproduced with permission.[88] Copyright 2020, Wiley-VCH.

PEDOT:EVA film as the adhesive between the flexible substrate and the perovskite (Figure 5c).[86] i) PEDOT:EVA can be used as a hole transport layer (HTL) between ITO and perovskite film; ii) PEDOT:EVA promotes the vertical crystallization of perovskite on flexible substrates to obtain high-quality perovskite films; iii) due to the good adhesion of EVA, it can connect brittle ITO and perovskite to improve flexibility. The PCE of the final device was as high as 19.87%. After a bending radius of 3 mm was applied for 7000 bending cycles, the device performance was still 85% of the initial value (Figure 5d). In addition, after the bending angle of the device reaches 60°, the device PCE can still recover more than 95% of the initial value, and the PCE continued to decrease until the bending angle was increased.

Previous reports have shown that net tensile stress causes the perovskite film to fracture, which will cause a series of parallel vertical channel cracks (approximately equidistant) in the metal halide perovskite film. These cracks do not affect the PCE of PSCs. However, these original cracks will provide a vertically free surface for the nucleation and propagation of more dangerous horizontal cracks at the perovskite interface, which significantly reduces the PCE. Grooves at the grain boundary and facets on the top surface of the perovskite film are usually early cracks, which can also be used as a focal point for reducing the brittleness of the perovskite. Recently, Shi's group grew in situ low-dimensional metal halide perovskite on the surface of perovskite as a surface passivation layer,[87] which not only reduced the tendency to fracture during bending but also provided protection against environmental species. First, excess PbI_2 was added to the perovskite precursor solution. After the perovskite film was annealed, the excess PbI_2 was deposited on the surface of the perovskite. Afterward, the 3-chlorobenzylammonium iodide (3-CBAI) solution was spin-coated on the surface of the perovskite and reacted with excess PbI_2 to form a low-dimensional perovskite. This layer of low-dimensional perovskite greatly enhanced the mechanical stability of the perovskite film. In contrast, the uncorrected perovskite film showed cracks and fractures. Under the test conditions of a bending radius $R = 5$ mm for 2000 cycles in ambient air (70% RH, 25 °C), the corrected perovskite film did not appear to be broken. In addition, this layer of low-dimensional perovskite adjusted the position of the top of the perovskite

© 2022 Wiley-VCH GmbH

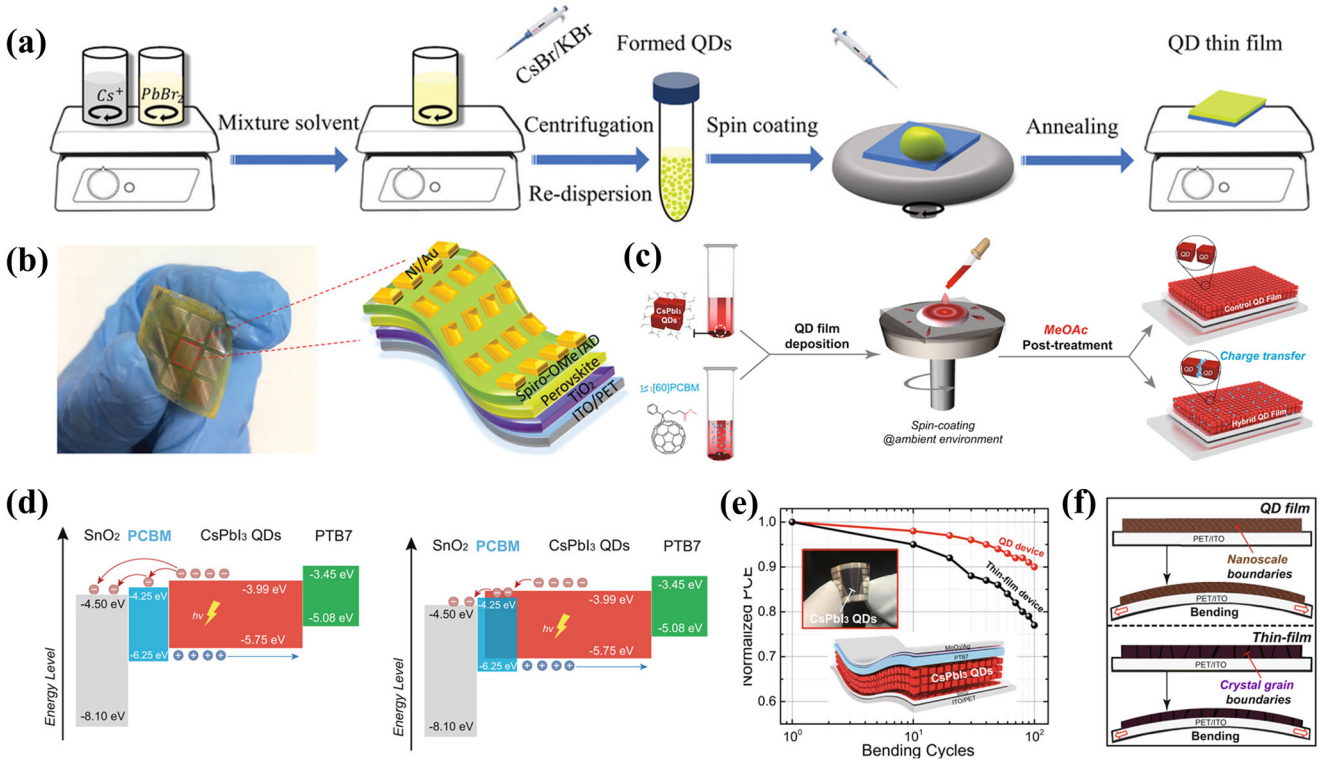


Figure 6. a) Schematic diagram of the synthesis process of CsBr/KBr-treated $CsPbBr_3$ quantum dots. b) Image of the flexible photodetector array (left) and schematic diagram of the device architecture (right). Reproduced with permission.[90] Copyright 2020, Wiley-VCH. c) Schematic diagram of the fabrication of $CsPbI_3$ QD films. d) Energy level diagrams for control and target devices. e) PCE as a function of bending cycles. The inset is the photograph of the flexible QD solar cell. f) Schematic diagram of bending mechanics testing of QDs and films on flexible substrates. Reproduced with permission.[91] Copyright 2020, Nature.

valence band and matched the energy level of the HOMO of the HTL more closely, which was conducive to the transport of photogenerated carriers. As a result, the flexible PSC of the modified perovskite film showed unprecedented bending durability. After 20 000 cycles, 81% of the initial PCE was retained at a bending radius of 5 mm in ambient air (≈ 20% RH, ≈ 25 °C). The improvement in the flexibility of the device is mainly attributed to the low-dimensional perovskite functioning to seal the surface defects of the perovskite. In summary, an effective way to improve the mechanical stability of the device is by increasing the contact between the perovskite and the substrate or the charge transport layer and passivating perovskite surface defects to reduce the effective early crack size through interface engineering.

In addition to improving the quality of the perovskite film and increasing the contact of the perovskite with other parts, the flexibility of the device can also be increased by adjusting the device structure. For example, our group fabricated flexible PPDs with a nested inverse opal (NIO) structure by using a polystyrene (PS) microsphere-assisted template method.[88] On the one hand, it is conducive to light capture; on the other hand, it is beneficial for pressure release. The optimum performance of $R = 473$ mA W^{-1} at 720 nm and $D^* = 1.35 \times 10^{13}$ Jones was obtained. To explore the reasons for the improvement in the mechanical stability of the device, finite element simulation is used to detect the stress distribution in the perovskite film. The results showed that the pressure distribution in a NIO structure film was more uniform and only 0.113 MPa, while the maximum stress in the flat film was 0.356 MPa (Figure 5e). The morphology of the NIO structure film was basically unchanged after bending; however, the planar film had cracks (Figure 5f). Finally, the light response of the device with the inverse opal structure was basically unchanged after 500 bending cycles. In contrast, after the planar device experienced 200 bending cycles, the optical response dropped to 69% of the initial value.

2.3.3. Low-Dimensional Structured Perovskite

Low-dimensional nanostructured perovskites, including 0D quantum dots (QDs), 1D nanowires (NWs), 2D nanosheets (NSs), etc., are very suitable for the preparation of flexible optoelectronic devices due to their unique low-dimensional structure, excellent optoelectronic properties, and mechanical stability.[89] Perovskite QD materials have excellent mechanical flexibility and are very suitable for the preparation of wearable devices. However, high-quality QDs usually require high-temperature and complex preparation processes, which conflict with the simple and cost-effective assembly concept of perovskites. Wu's group used the following method, which does not require high temperatures and complicated synthesis processes: CsBr/KBr assisted $CsPbBr_3$ QD growth (**Figure 6**a).[90] The R and D^* values of the optimized device reached 10.1 A W^{-1} and 9.35×10^{13} Jones,

© 2022 Wiley-VCH GmbH

which were increased by more than 300% and more than 1000%, respectively. The arrays had obvious folding resistance, electrical stability, and performance uniformity (Figure 6b). The results showed that even after 1600 bending cycles, the dark current and photo current maintained 93% of the initial value, indicating that the device had strong flexural resistance and electrical stability. However, the performances of flexible devices based on perovskite QDs were generally inferior to that of flexible organic thin-film solar cells, which may be due to QD heterojunctions and poor interface charge transfer capabilities. Recently, Wu's group incorporated phenyl-C61-butyric acid methyl ester (PCBM) into the perovskite layer (Figure 6c),[91] in which PCBM bonded the uncoordinated Pb^{2+} ions on the QD surface through functional carboxyl groups and formed a bond between the $CsPbI_3$ QD layer and the ETL tin oxide. PCBM inhibited charge recombination at the interface of the QDs and SnO_2 (Figure 6d). An exciton cascade achieved a champion efficiency of 12.3% for flexible substrate and better mechanical flexibility. The test results showed that after 100 bending cycles with a bending radius of 0.75 cm, the QD device retained 90% of the initial value, while the efficiency of the $CsPbI_2Br$ film was only ≈75% of the initial efficiency (Figure 6e). Moreover, even if the number of bending cycles ranged from 100–1000 cycles, the morphology remained basically unchanged (Figure 6f), so the degradation of the device performance was mainly due to the destruction of the ITO and Ag electrodes.

Compared with thin films, perovskite NWs generally have better flexibility. Therefore, various flexible devices based on perovskite NWs have been prepared. $CsPbI_3$ exhibits an orthorhombic structure at room temperature. $CsPbI_3$ is composed of 1D PbI_6 octahedrons, and cesium atoms are bonded through ionic bonds,[92] which indicates that $CsPbI_3$ prefers to grow into NWs. Therefore, $CsPbI_3$ NWs can be easily grown on rigid and flexible substrates through a one-step self-assembly solution process. After annealing at 60 °C, excess solvent is removed.[93] Because no high temperatures are used in the whole preparation process, the device based on $CsPbI_3$ NWs has better flexibility, and the optical flow anisotropy ratio of the device is only reduced by 5% after 500 bending cycles. However, the existing nanomanufacturing methods lack the ability to control the quantity, location, direction, and quality characteristics of the perovskite NWN, and the growth mechanism is still unclear. Kim's group demonstrated a micro/nanofluidic fabrication technique (MNFFT) that can precisely control and monitor the growth of perovskite NWN on site (**Figure 7**a).[94] The nanochannel guides the nucleation point and growth path of the $MAPBI_3$·DMF NW array (NWA). In situ UV spectra and absorption spectra were measured in real time to study the growth mechanism of DMF-mediated $MAPbI_3$ crystals. This solution-mediated crystallization is also one of the most common chemical phenomena in nature. After that, this group grew $MAPbI_3$ NWA on the PET substrate by using MNFFT technology to connect PDMS film with nanochannels. The NWA-based device had good flexibility, and the light-dark current did not change significantly after 2000 bending cycles with a bending diameter of 10 mm (Figure 7b,c).

In the two methods mentioned above, NWs need to be grown on templates, and the nanostructured substrate cannot be reused. The imprinting method is another effective method for preparing ordered nanowire arrays. The template used for imprinting can be reused, and the imprinting method has no special requirements for the substrate. Our group used DVD as a template for imprinting to prepare a highly ordered array of NWs (Figure 7d).[95] PPDs based on nanowire arrays usually have a planar metal-semiconductor-metal structure, which means that the device can only work under an external bias, which is not conducive to the practical application of the device. Therefore, ferroelectric poly(vinylidene-fluoride-trifluoroethylene) (P(VDF-TrFE)) was added to the perovskite precursor solution, which enhanced the ferroelectricity of the active layer. Therefore, after a certain polarization bias is applied, the device can still work without an external bias. In addition, the device had good flexibility. When the angle of intersection between the bending direction and the nanowire array direction is set to 0°, the photocurrent remains unchanged. The photocurrent did not change significantly after the bending angle changed from 0° to 180° or after 200 bending cycles. Later, our group prepared a self-powered flexible detector based on NWA with the aid of $CsPbI_3$-$CsPbBr_3$ heterojunction construction (Figure 7e).[96] Under normal circumstances, it is impossible for a device based on a uniform nanowire array to have a photoresponse when there is no external force. However, our group achieved the self-driven phenomenon by constructing a heterojunction. First, by controlling the concentration of the perovskite precursor solution and the amount of polyvinylpyrrolidone (PVP) additive, $CsPbI_3$ NWAs were prepared by the imprinting method. Subsequently, half of the $CsPbI_3$ was converted into $CsPbBr_3$ by the gas phase ion exchange method. Then, at the boundary between $CsPbI_3$ and $CsPbBr_3$, an Ag wire with a diameter of 50 μm was fabricated. After Au electrodes were fabricated by thermal evaporation equipment, a self-powered device based on a $CsPbI_3$-$CsPbBr_3$ NWA heterojunction was successfully fabricated. The results showed that the *R*-value reached 125 mA W^{-1}, and the rapid rise and decay times reached 0.7 and 0.8 ms, respectively, without external bias. In addition, the device also had good flexibility. The photocurrent of the device remained above 90% after 100–500 bending cycles, and the photocurrent was basically unchanged after a bending angle from 0–180° was applied.

Compared with single NWs or NWAs, the simple preparation process of nanowire NWNs enables them to be used in large-scale, flexible, and wearable PPD applications.[97] However, there are many microinterfaces (MIs) between the NWs in an NWN, which severely limits the performance and stability of the device. This is because these MIs bring some instability factors. First, the MIs between NWs hinder carrier transmission. Second, the easy adsorption of water and oxygen at the micro interface is not conducive to stability. Third, due to the unbalanced tension of the upper and lower layers of an NWN, the NWN easily breaks during the bending process, which is not conducive to flexibility. Therefore, Zeng's group demonstrated a $MAPbI_3$ NWN welding strategy, which adopted a pressure-assisted annealing process (PAAP).[97] It was shown that NWs grew secondary, from the contact area between NWs, leading to the disappearance of MIs because $MAPbI_3$ NWN was covered by glass and processed by PAAP. In addition, it enhanced the crystallinity of the NWN and enhanced the radial transmission of the light source carriers, thereby obtaining better device performance. The results showed that the NWN prepared under the conditions of 100 °C and 2.7 MPa had the best morphology. The device had an on/off

© 2022 Wiley-VCH GmbH

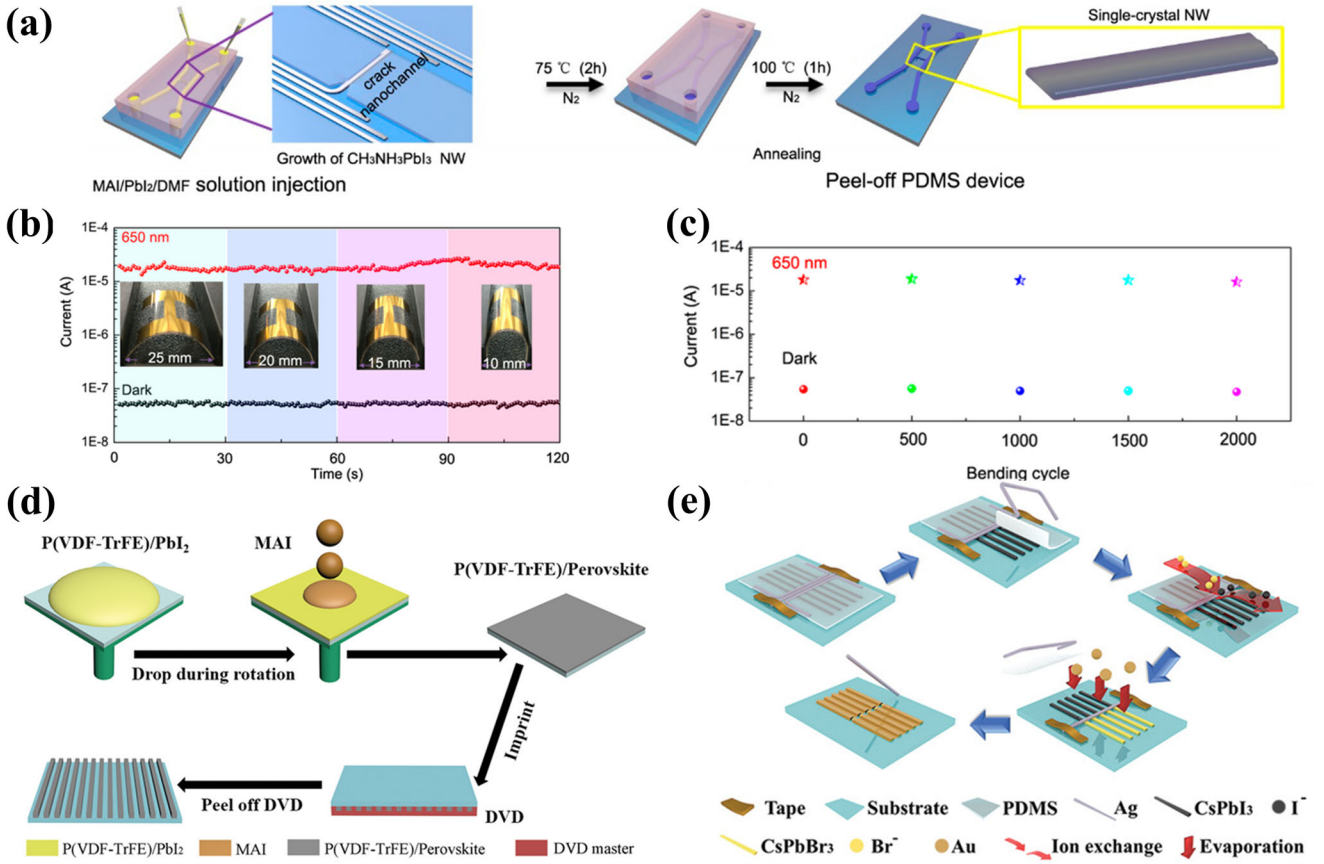


Figure 7. a) Schematic of the solution-mediated fabrication method for a $MAPbI_3$ NW. b) The current of flexible photodetectors bent to different radii with a bias voltage of −5 V. Middle insets show corresponding photographs of the device under the four bending conditions. c) Photocurrent and dark current with different bending cycles. Reproduced with permission.[94] Copyright 2018, American Chemical Society. d) Schematic diagram of the fabrication of perovskite nanowires using the DVD imprinting method. Reproduced with permission.[95] Copyright 2019, Wiley-VCH. e) Schematic diagram of the fabrication of perovskite nanowires using the PDMS imprinting method. Reproduced with permission.[96] Copyright 2020, Wiley-VCH.

current ratio of 2.8×10^4 and a D^* of 4.16×10^{12} Jones, which can be compared with a single NW or NWA PPD. Moreover, unpackaged NWN PPDs had good stability in air with a humidity of 55–65%, and the performance of the device was basically unchanged after 250 bending cycles under different bending radii and 1000 bending cycles under a fixed bending radius. These results showed that the welding strategy greatly improved the performance of NWA flexible devices.

In addition to 0D QDs and 1D NWs, low-dimensional perovskite structures also include 2D NSs. Zeng's group combined conductive CNTs with $CsPbBr_3$ NSs,[98] which greatly improved the device performance. This was because CNTs not only effectively promoted the extraction of photogenerated carriers but also greatly reduced the film resistance to provide a fast transport channel for the carriers. The *R*, EQE, and response speed of the final device were greatly improved. In addition, due to the nanosheet structure of $CsPbBr_3$ and the NB structure of CNTs, the device had good flexibility, and the device did not change significantly under different bending radii. Under a bias of 3 V, the photocurrent maintained 93.6% of the initial value after 10 000 bending cycles.

In summary, to achieve high-performance flexible PSCs and PPDs, researchers have performed much work on substrate selection, electrode design, and perovskite layer engineering. The main advantages and disadvantages of the various flexible components mentioned above are summarized in **Table 1**. Till now, perovskite polycrystalline film format has been intensively studied and already yielded a large number of flexible PPDs and PSCs. Unfortunately, abundant defects in polycrystalline films restrict the device performance. Owing to their absence of grain boundaries, low trap densities, and large carrier mobilities, perovskite single crystals are expected to achieve impressive performances. However, perovskite single crystals are not suitable for making flexible devices because of their fragility. The single crystal should be thin enough to have a certain degree of mechanical flexibility. The perovskite layer with superior mechanical stress tolerance will enable the device less affected by bending stress, thus retaining the original performance of the device. In comparison to perovskite polycrystalline film and single crystal, low-dimensional perovskite exhibits higher tolerance to film cracks and better mechanical stability, thus making it an ideal candidate for flexible perovskite devices.

© 2022 Wiley-VCH GmbH

Table 1. Advantages and disadvantages of different flexible materials.

	Part	Material	Advantage	Disadvantage
Flexible PSCs/PPDs	Substrate	Polymer substrate (PI, PET, PEN)	Flexibility, great stability, excellent transparency	Expensive, not resistant to high temperature, limited flexibility
		Carbon cloth, carbon fiber	Low cost, good flexibility	Complex device fabrication process
		Paper	Green, nonpolluting, degradable, foldable, and lightweight material,	Easy to tear
		Mica	Good transparency, high heat resistance, excellent mechanical flexibility, abundant reserves, and easy processing characteristics	-
		Flexible glass	High transparency, high temperature resistance, and chemical stability	High thickness requirement
		Metal (Ti)	High flexibility, conductivity, and excellent high temperature resistance	High thermal expansion coefficient
	Electrode	Metal	Good compatibility	Expensive, vacuum preparation
		Graphene	High carrier mobility, good chemical stability, and good mechanical flexibility	Mismatched energy levels
		Metal oxide electrodes	Poor flexibility	High-temperature sputtering
	Perovskite	Single crystal	High absorption coefficient, long carrier lifetime, large carrier mobility, low defect state density, and high defect tolerance	High thickness requirement
		Polycrystalline perovskite film	Simple preparation process and low cost	General flexibility
		Low-dimensional structure perovskite	Good flexibility and low requirements for the device structure	Complex preparation process

3. Semitransparent PPDs and PSCs

Ideal semitransparent devices can transmit a portion of visible light or near-infrared light while absorbing light energy to ensure a certain light transmittance.[17,18] Semitransparent photovoltaic devices can be used as windows in buildings and skyscrapers to provide shade (through visible light) and green electricity for buildings[99,100] and can be made into series devices with other mature photovoltaic devices to obtain higher performance (through near-infrared light).[101–103] For example, most solar cells are built in open spaces or high locations to absorb more sunlight, while semitransparent cells can be built on both sides of the building, which not only saves space but also provides a certain amount of shadows. Si-based solar cells can absorb near-infrared light, but most of Pb-based PSCs cannot. Therefore, combining Si-based cells with Pb-based PSCs can break Shockley-Queisser limits. Most silicon-perovskite tandem solar cells are connected in series with four terminals (usually involving the mechanical stacking of the semitransparent perovskite top cell on the silicon bottom cell) or two-terminal series (including monolithic integration of the perovskite top cell with the silicon bottom cell). To date, the efficiencies of four-terminal and two-terminal silicon perovskite tandem solar cells have exceeded 27% and 29%, respectively.[104,105] The high transparency of the perovskite cell is beneficial for light to pass through the top perovskite cell and reach the bottom silicon bottom cell, which is essential for high-performance integrated devices. It is generally believed that an average visible transmittance (AVT) (380–780 nm) higher than 20% is the minimum standard for semitransparent cells,[106–108] which means that there are certain requirements for the light transmittance of each component of the photovoltaic device, such as the active layer (perovskite) and electrode layer. **Figure 8** depicts a timeline of representative works on semitransparent devices, and these works mainly focused on optimizing the electrode and perovskite layer. Therefore, the following part will mainly discuss and summarize the design strategies to achieve semitransparent PSCs and PPDs.

3.1. Electrode

Traditional semitransparent devices use metals with a thickness of tens of nanometers or even close to 100 nanometers as electrodes, but for semitransparent photovoltaic devices, such a thickness makes it difficult to transmit visible light. To prepare a semitransparent device, it is necessary to process the electrodes. Generally, there are two treatment methods. One is to use transparent oxide instead of metal electrodes; the other is to make the metal electrodes thin enough to allow part of the visible light to pass through.

A good semitransparent electrode should have the following characteristics: i) it has no physical or chemical reaction with the perovskite and charge transport layer below; ii) it allows more incident light to pass through. and iii) it has good charge collection conductivity. Unfortunately, transparent oxide electrodes, such as SnO_2, zinc tin oxide (ZTO), TiO_2, ZnO, Al-doped ZnO, and indium-doped ZnO (IZO), are usually deposited by magnetron sputtering, which not only requires higher pressure and temperature but also damages the underlying perovskite layer and organic interface layer. Although there have been some reports on damage-free sputtering methods, the film conductivity is still very low. Thin films with higher electrical conductivity and

© 2022 Wiley-VCH GmbH

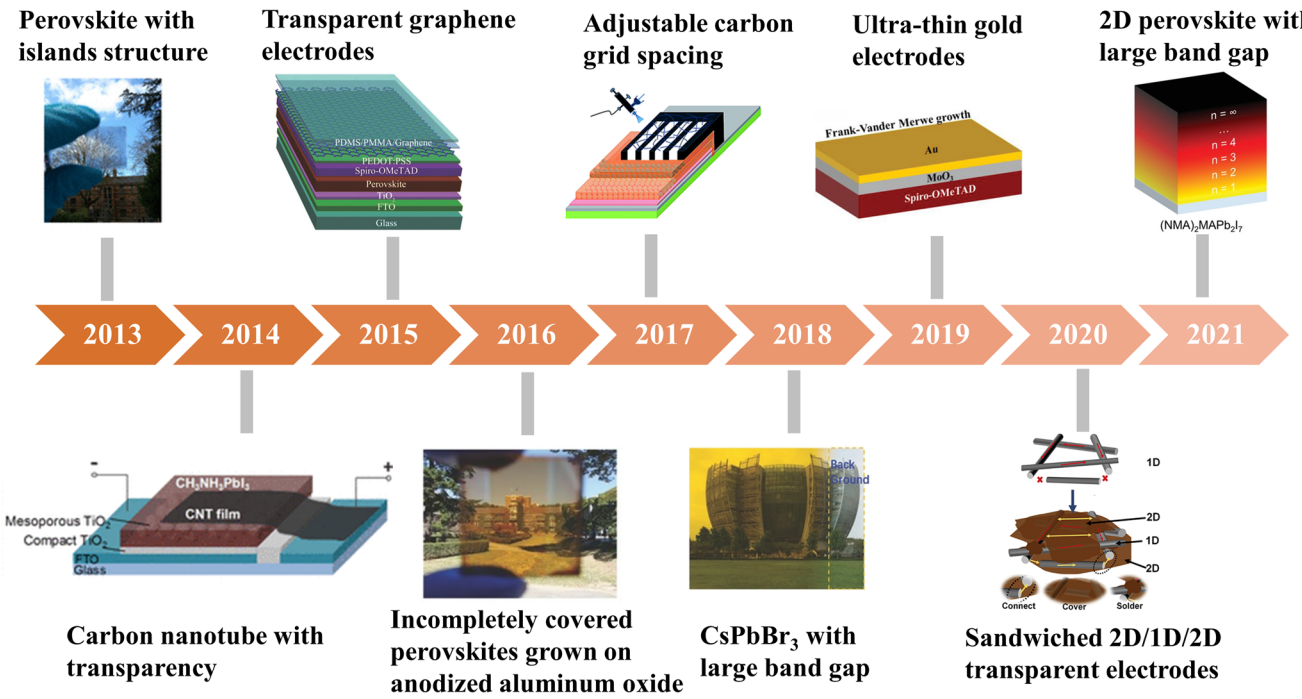


Figure 8. A timeline of representative works on semitransparent PSCs and PPDs. Perovskite with island structure. Reproduced with permission.[46] Copyright 2013, American Chemical Society; Carbon nanotube with transparency. Reproduced with permission.[99] Copyright 2014, American Chemical Society; Transparent graphene electrodes. Reproduced with permission.[17] Copyright 2015, Wiley-VCH; Incompletely covered perovskites grown on anodized aluminum oxide. Reproduced with permission.[122] Copyright 2016, Wiley; Adjustable carbon grid spacing. Reproduced with permission.[18] Copyright 2017, The Royal Society of Chemistry; $CsPbBr_3$ with large band gap. Reproduced with permission.[123] Copyright 2018, Wiley-VCH; Ultra-thin gold electrodes. Reproduced with permission.[116] Copyright 2020, Wiley; Sandwiched 2D/1D/2D transparent electrodes. Reproduced with permission.[107] Copyright 2020, Elsevier Ltd.

light transmittance often require harsher ITO sputtering conditions, such as higher sputtering power. Therefore, a buffer layer is needed to avoid negative effects on the perovskite layer. Due to the limited heat resistance of perovskite, the deposition process of the upper film requires low temperature, and the resulting film has the advantages of high mobility, high transmittance, and a pinhole-free morphology. The commonly used oxide buffer layer is MoO_3, but it has a large sheet resistance and easily reacts with perovskite, which is not conducive to long-term stability.[109–111] Therefore, it is important to develop other sputtering buffer materials that not only protect the bottom layer but also ensure high device efficiency.

Seo's group microprocessed with NbO_y, which restored the fill factor from 70.4% to 80.3%,[112] and the PCE reached more than 18% (**Figure 9**a). By using a silicon cell with an efficiency of 22.9%, the total efficiency of the four-terminal series structure reached 26.0%. WO_x played the role of a protective layer, and NbO_y improved the morphology of WO_x and finally effectively improved the fill factor of the device. The corresponding cross-sectional SEM image of the whole device is shown in Figure 9b. Because the film is extremely thin, the thin film shows excellent transmittance, which is >95% (Figure 9c), in the whole visible and near infrared wavelength range. In addition, the reflective film increased the short-circuit current. Soon after, Hoye's group used p-type CuO_x as a buffer layer for the first time because CuO_x can be deposited at a temperature below 200 °C by ALD technology to avoid damage to the hole transport material.[113] Cu_xO has high transmittance and hole mobility. The research results showed that deposition at 100 °C did not damage the perovskite layer but affected the carrier transport kinetics. Moreover, it effectively blocked the damage of perovskite and PTAA caused by ITO sputtering of the transparent electrode. The best performance of the final device was 16.7%. The efficiency of the four-terminal series structure was 24.4%.

When the metal is thin enough, it can also function as a transparent electrode. However, the coupling strength between Au atoms is usually stronger than that of the substrate, which leads to the formation of Au islands through Volmer-Weber growth during the thermal evaporation process, and a continuous ultrathin film cannot be obtained. Therefore, continuous ultrathin metal films are desirable, and some measures can be taken to obtain them. For example, Huang's group induced continuous Au ultrathin film production with 1 nm Cu (Figure 9d).[114] The 1 nm of Cu improved the wettability of Au. Au atoms preferentially adhered to the Cu surface rather than to each other, leading to the growth of Frank-van der Merve and the formation of a continuous ultrathin Au film. The highest light transmittance of this composite film was close to 70% (Figure 9e). The final semitransparent device performance reached 16.7%, and the PCE of the tandem device combined with the infrared-enhanced silicon heterojunction cell specially adjusted for the perovskite/silicon tandem device reached 23% (Figure 9f). It is worth noting that the light transmittance of Cu in the near-infrared light region is not ideal, which will affect the performance of the series cir-

© 2022 Wiley-VCH GmbH

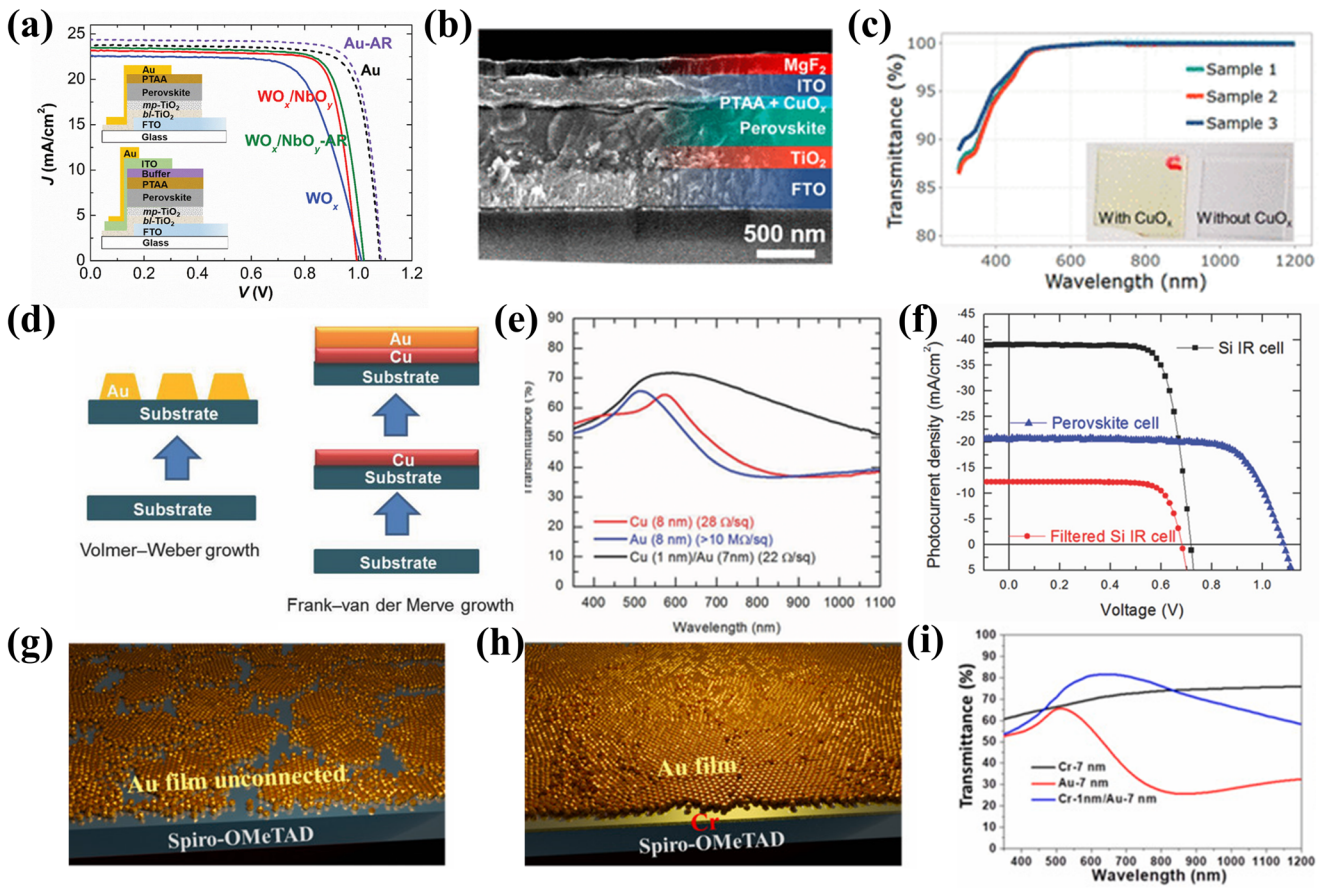


Figure 9. a) Current density versus voltage (*J*–*V*) of PSCs. The insets are the structure of semitransparent devices with untreated and treated buffers. Reproduced with permission.[112] Copyright 2020, Wiley-VCH. b) Cross-sectional scanning electron microscopy image of the semitransparent device. c) Corresponding measured transmittance. The inset shows photographs of borosilicate glass with (left) and without (right) the CuO_x layer. Reproduced with permission.[113] Copyright 2020, American Chemical Society. d) Growth of Au on glass substrates (left) and copper-coated glass substrates (right). e) Transmittance and conductivity of the corresponding films. f) *J*–*V* curves of three batteries. Reproduced with permission.[114] Copyright 2016, Wiley-VCH. SEM images of Au grown on g) spiro-OMeTAD and h) Cr substrates. i) Transmittance of corresponding films. Reproduced with permission.[115] Copyright 2021, Elsevier Ltd.

cuit with the Si battery. As shown in Figure 9g, h, Priya's team prepared an ultrathin Au metal electrode with a continuous distribution by introducing a Cr seed layer, which improved the efficiency of semitransparent perovskite devices and tandem solar cells.[115] The results showed that the Cr/Au electrode had good transmittance (Figure 9i), and the PCE of semitransparent PSCs reached 19.8%. They used COMSOL to simulate the light field distribution and demonstrated that the semitransparent PSCs had a higher light transmittance in the near-infrared band. Finally, the PCE was as high as 28.3% a semitransparent perovskite-type top cell mechanically superimposed on the tandem solar cell on the bottom cell of the silicon heterojunction was used. In addition to the use of metals as materials for inducing ultrathin Au film growth, MoO_3 is another option. Yang's team designed an electrode with a MoO_3/Au/MoO_3 structure.[116] Due to its large surface tension (≈ 200 mN m^{-1}), the MoO_3 at the bottom formed an ultrathin layer of Au on the surface of the molybdenum oxide by means of a thermal evaporation membrane (**Figure 10**a,b). The device had good transmittance (Figure 10c). In the wavelength range of ≈800–1100 nm, when the thickness of the top MoO_3 was 80 nm, the lowest average transmittance was ≈74%, and there was a lower reflectivity in the visible and infrared regions. The presence of MoO_3 significantly increased the offset between the electron and HTL, which was beneficial to reduce charge recombination and energy loss, resulting in a higher V_{OC} for semitransparent devices (Figure 10d). As a result, the semitransparent PSCs showed an efficiency of 18.3%. When the semitransparent perovskite device was mechanically stacked with a 23.3% PCE heterojunction silicon solar cell, its overall efficiency was 27.0%, which was higher than that of the two subcells. Therefore, the introduction of inducers with large surface energy to induce the growth of Au ultrathin films is an effective strategy for preparing transparent metal electrodes.

In addition to sufficiently transparent ultrathin metal, metal NWs can also be used as transparent electrodes. Metal NWs are a promising type of transparent electrode that can be processed by liquid dispersion at low temperature. Ag NWs can be dispersed in alcohol or water. However, water severely destroys the stability of the Pb halide, and the stability of metal NWs is an issue. Therefore, a protective layer is essential. At the same time, the

© 2022 Wiley-VCH GmbH

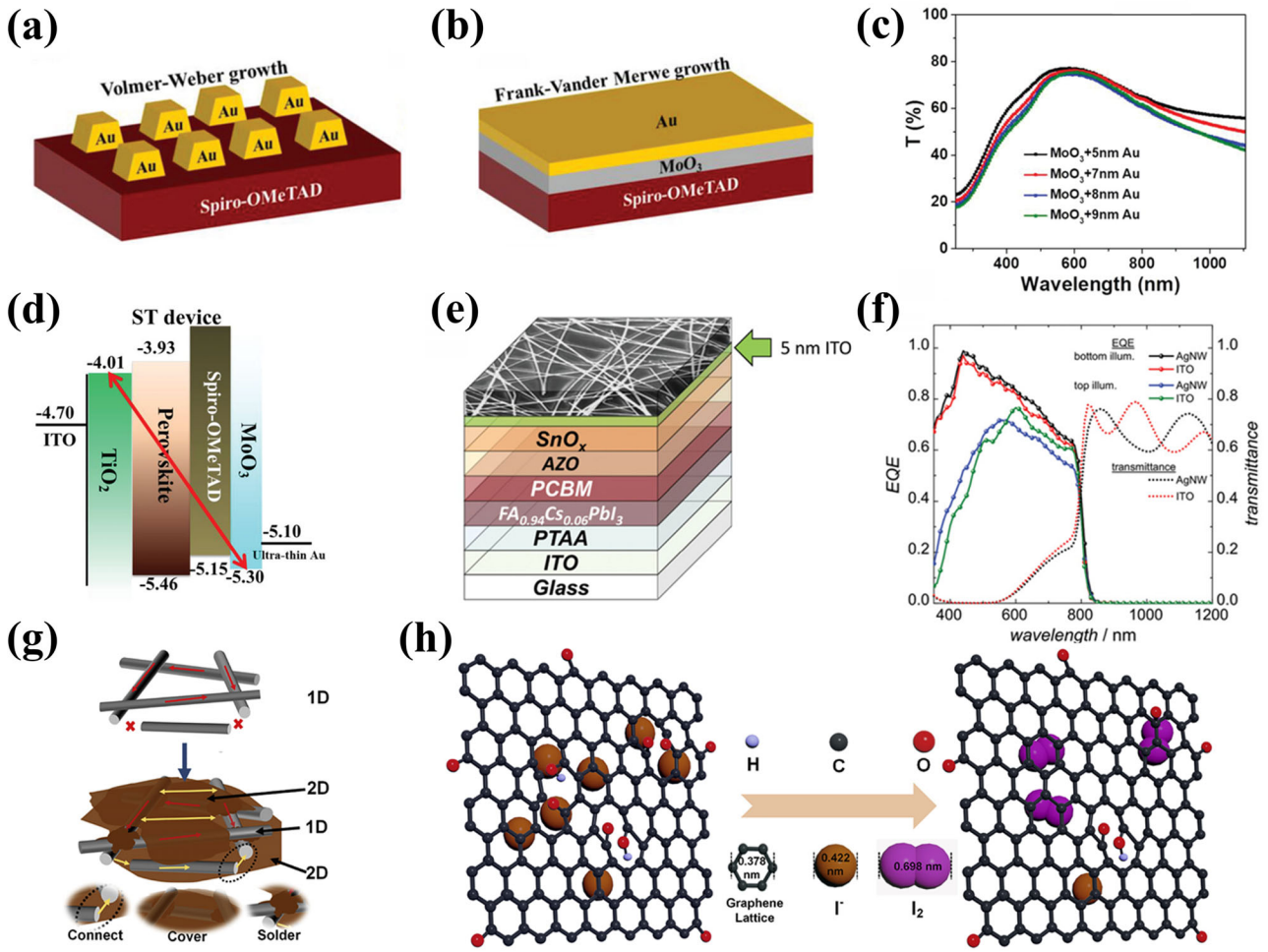


Figure 10. Illustration showing the growth of Au on a) spiro-OMeTAD and b) MoO_3 substrates. c) Transmittance spectra for gold layers deposited on MoO_3 substrates. d) Energy level alignments of semitransparent perovskite devices. Reproduced with permission.[116] Copyright 2020, Wiley-VCH. e) PSC stacks used to test the impact of water exposure with an ALD-grown SnO_x layer. f) EQE (straight lines) and transmittance spectra (dotted lines) for the respective cells. Reproduced with permission.[117] Copyright 2020, Wiley-VCH. g) Schematic diagram of 1D/2D/1D materials. h) Schematic diagram of the graphene-enhanced iodide ion blocking effect. Reproduced with permission.[107] Copyright 2020, Elsevier Ltd.

protective layer can be used as an electronic interface between the device and the Ag NWs (Figure 10e). The protective layer of the ETL is composed of a layer of aluminum-doped ZnO and a dense SnO_x layer grown by low-temperature ALD, which provides effective protection for perovskite waterproofing.[117] PVP acts as a capping agent for Ag NWs, causing a work function shift between SnO_x and Ag NWs. This problem is solved by inserting a layer of 5 nm ITO between the two. The final semitransparent device PCE reached 17.4% upon illumination from the bottom (substrate) side and 13.4% for top-side illumination, which was higher than PSCs with ITO as the electrode. Moreover, the average light transmittance of the device in the 550–820 nm region was 16%, and the average light transmittance of the near infrared (>820 nm) region was 68% (Figure 10f). This work also paves the way for the production of more environmentally friendly and lower-cost single-junction and multijunction PSCs in the future.

In addition, Zhong's group formed a 2D/1D/2D sandwiched electrode by encapsulating 1D Ag NWs in 2D graphene NSs (Figure 10g), thus improving the stability of the device.[107] Flakes of graphene NSs can be brazed and wound with Ag NWs, enhancing the contact between NWs, which greatly improves the electrical conductivity. Moreover, because the size of I^- ions (0.422 nm) was larger than the hexagonal lattice framework (0.378 nm), I^- ions cannot pass through the intact graphene film. Furthermore, I^- ions can induce graphene lattice repair for self-enhanced iodine blocking (Figure 10 h). This device with a unique structure has favorable performance and stability.

For PPDs with photoconductor device structure, there is a certain space between the two electrodes of the device; it is not full coverage like the electrode of the vertical device. Thus, the device with this structure has a certain light transmittance ability. When the perovskite film is not particularly thick and the substrate is transparent, the device is a semitransparent device. PPDs with photodiode structures, since they have the same structure as PSCs, have similar research paths. Blink's group demonstrated the first translucent near-infrared PPD using mixed tin lead perovskite as the active material. The device consisted of a perovskite active layer sandwiched between two transparent ITO electrodes.

© 2022 Wiley-VCH GmbH

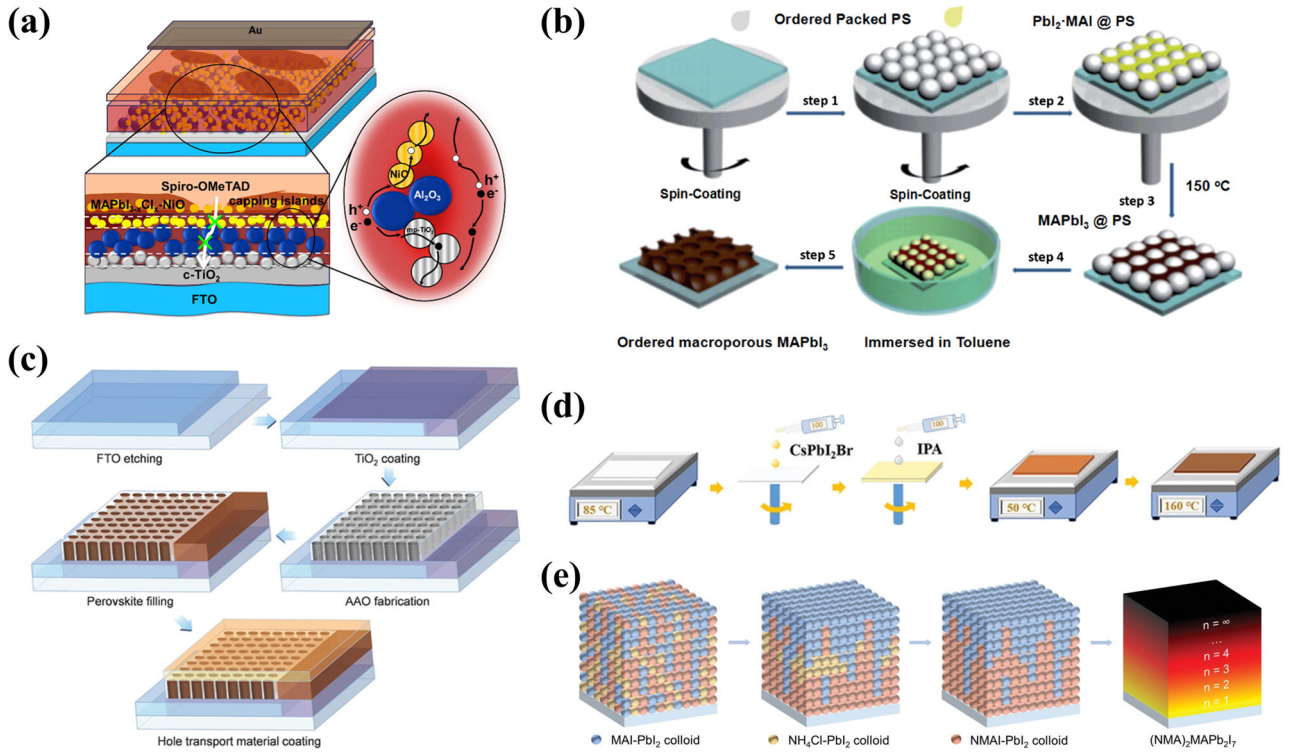


Figure 11. a) Schematic diagram of the device structure and barrier properties based on island-structure-$MAPbI_{3-x}Cl_x$. Reproduced with permission.[120] Copyright 2018, Elsevier Ltd. b) Schematic illustration of the flow sheet for the preparation of macroporous (MP) perovskite thin films on bl-TiO_2 using sacrificial PS templates. Reproduced with permission.[121] Copyright 2016, The Royal Society of Chemistry. c) Schematic diagram of preparing perovskite based on AAO template. Reproduced with permission.[122] Copyright 2016, Wiley-VCH. d) Schematic diagram showing the preparation of $CsPbI_2Br$. Reproduced with permission.[125] Copyright 2021, Wiley-VCH. e) Schematic illustration of the formation of graded 2D perovskite films. Reproduced with permission.[126] Copyright 2021, Wiley-VCH.

The top electrode was processed by pulse layer deposition, and there was no visible damage to the perovskite layer below. The transparency of the whole device in the near-infrared spectrum range exceeded 48%. The photodetector showed a dark current of 1.74×10^{-2} mA cm^{-2} at −0.2 V, with the external quantum efficiency of 23% and 13% and D^* of 6.6×10^{10} and 4.2×10^{10} Jones at 850 and 940 nm, respectively.[118] Graphene is widely used in electrodes. Sun's group used chemical vapor deposition to grow high-quality single-layer graphene, and developed a new type of transparent graphene electrode organic inorganic halide PPD with wide spectral response. The on/off ratio of the device was as high as 10^6, and the device had a broad spectral response ranging from UV–visible to near-infrared. At the same time, it had excellent detection ability for weak light. Using a transparent graphene electrode, it can work on both sides, the LDR values on both sides of the device were higher than 100 dB. Response time was less than 10 μs.[119] Their semitransparent characteristics and unique photoelectric detection function will provide new applications for the daily life.

3.2. Active Layer

In addition to highly transparent electrodes, semitransparent devices also require highly transparent perovskite films. Some options to achieve this goal are as follows: i) reduce the perovskite coverage, ii) decrease the perovskite thickness, and iii) adjust the band gap of the perovskite.

3.2.1. Reduce Perovskite Coverage

A discontinuous perovskite film has high light transmittance due to the voids in the film. Hahn's group used a discontinuous island structure of an $MAPbI_{3-x}Cl_x$-NiO composite film as a light-absorbing layer to prepare an FTO/c-TiO_2/mp-TiO_2/Al_2O_3/NiO/$MAPbI_{3-x}Cl_x$-NiO/Spiro-OMeTAD structured device (**Figure 11**a).[120] The discontinuous $MAPbI_{3-x}Cl_x$-NiO film was obtained by controlling the rotation speed. This is because most of the $MAPbI_{3-x}Cl_x$-NiO solution is removed during high-speed rotation, and it is difficult to form a uniform and dense perovskite film when the remaining solution amount is very small. Such a film had a high light transmittance, but this in turn resulted in a lower short-circuit current. Therefore, the existence of Al_2O_3/NiO interface engineering inhibited interface recombination, resulting in a higher short-circuit current. The PCE of the final semitransparent device was 10.06%, and the AVT was 27%. The PS microsphere template can also assist in the preparation of perovskite films with ordered macropores (Figure 11b).[121] By adjusting the concentration of the perovskite precursor solution and the diameter of the PS microspheres, the pore distribution of the perovskite film can be adjusted, and the

© 2022 Wiley-VCH GmbH

Table 2. Advantages and disadvantages of different semitransparent materials.

	Part	Material	Advantage	Disadvantage
Semitransparent PSCs/PPDs	Electrode	Transparent oxide electrodes	High transparency, good conductivity, suitable energy level	High temperature preparation
		Metal film	Good conductivity	Need to be thin enough; Ag, unstable, easy to diffuse; Au, expensive, uneven growth when too thin
		Ag NWs	Liquid dispersion at low temperature	A protective layer is required to protect the underlying perovskite from destruction
	Perovskite	Low perovskite coverage	High light transmittance	Leaks easily
		Thinner perovskite films	Increases the overall range of light transmission	Poor film quality
		Large band gap	Great transmittance in the infrared range	Low PCE

VAT can also be adjusted from 20% to 45%. In addition, anodic aluminum oxide (AAO) can also be used as a semitransparent perovskite layer prepared as a scaffold template because AAO can limit the distribution of perovskite (Figure 11c).[122] By controlling the aperture in the AAO, the volume occupied by the perovskite layer can be accurately changed, thus adjusting the light transmittance of the perovskite. In short, whether island-shaped perovskites are obtained by controlling the rotation speed or the spatial distribution of perovskites is controlled by the template method, the aim is to increase the light transmittance by reducing the distribution of perovskites.

3.2.2. Decrease Perovskite Thickness

The thickness of the perovskite film is inversely proportional to the light transmittance, so reducing the thickness of the film is an effective way to achieve semitransparent devices. When using the solution method to prepare thinner perovskite films, discontinuous films and large pores are disadvantages. Li's group used the dual-source vacuum coevaporation (DSVE) method to develop a high-quality $CsPbBr_3$ inorganic perovskite film with a thickness of 450 nm, which was obtained by controlling the stoichiometric ratio and evaporation rate of CsBr and $PbBr_2$.[123] The device not only exhibited an AVT of ≈60% in the visible region over 530 nm but also possessed an open-circuit voltage of 1.44 V. After that, Alberti's group used a completely solvent-free vacuum deposition method to prepare the photoactive $MAPbI_3$ layer.[124] In this method of depositing perovskites under low vacuum conditions, the chamber pressure and source-substrate distance become additional parameters to improve the perovskite quality, enabling a reduction in thickness without affecting the photovoltaic performance. Finally, with only an 80 nm thick active layer, the average efficiency of PSCs was 12.9%, the best efficiency was 13.8%, and the AVT value was 32.8%. In general, the key point to realize semitransparent devices by controlling the thickness of the perovskite film is to ensure the quality of the perovskite.

3.2.3. Adjust the Band Gap of Perovskite

Semitransparent devices can transmit a certain amount of visible light or near-infrared light; however, FA-based or MA-based perovskites usually have small band gaps and wide light absorption ranges, which lead to unsatisfactory light transmittance. $CsPbI_3$, $CsPbI_2Br$, $CsPbIBr_2$, $CsPbBr_3$, and other perovskites with large band gaps can transmit visible light or near-infrared light. For example, our group used $CsPbI_2Br$ with a large band gap of 1.9 eV as the active layer.[125] Generally, the quality of the $CsPbI_2Br$ film is poor, so (chloromethylene)-dimethylammonium chloride (CDCl) is used as an additive to form an intermediate adduct of PbI_2·CsBr·CdCl, which greatly improves the quality of the perovskite film (Figure 11d). The final PSCs exhibited PCEs of 14.01% and 10.36% under high AVTs of 31.7% and 40.9%, respectively.

Compared with 3D perovskites, 2D perovskites have larger band gaps and can also be used as the active layers of semitransparent devices. The 2D perovskite with n≥2 has a large band gap, high transmittance, and excellent stability. However, the exciton binding energy is not conducive to carrier separation, and the high electrical anisotropy structure hinders the out-of-plane charge transfer, resulting in a low PCE for 2D perovskite-based PSCs. Mazeeruddin's group prepared a 2D perovskite $(NMA)_2(MA)Pb_2I_7$, which was made of a low-*n*-value perovskite film, and its *n*-value gradually increased from bottom to top (Figure 11e).[126] In addition, ammonium chloride (NH_4Cl) was added to further strengthen the phase separation and promote good out-of-plane orientation. As a result, the semitransparent PCE was 7.52% under the high AVT of 40.5%. This work studies the new applications of a low average number of 2D perovskites in high-efficiency and stable semitransparent PSC applications and provides new ideas for other types of optoelectronic devices. In summary, a perovskite layer with a large band gap is conducive to the passage of more visible light, and on this basis, a certain performance is guaranteed. **Table 2** presents the advantages and disadvantages of the various materials and methods used to achieve semitransparent devices.

4. Self-Healing PPDs and PSCs

Over the past few decades, the performance of PPDs/PSCs has developed rapidly. However, the inherent instability of perovskite materials hinders their continued development. Perovskite is easily degraded by external environmental factors such as light, heat,

© 2022 Wiley-VCH GmbH

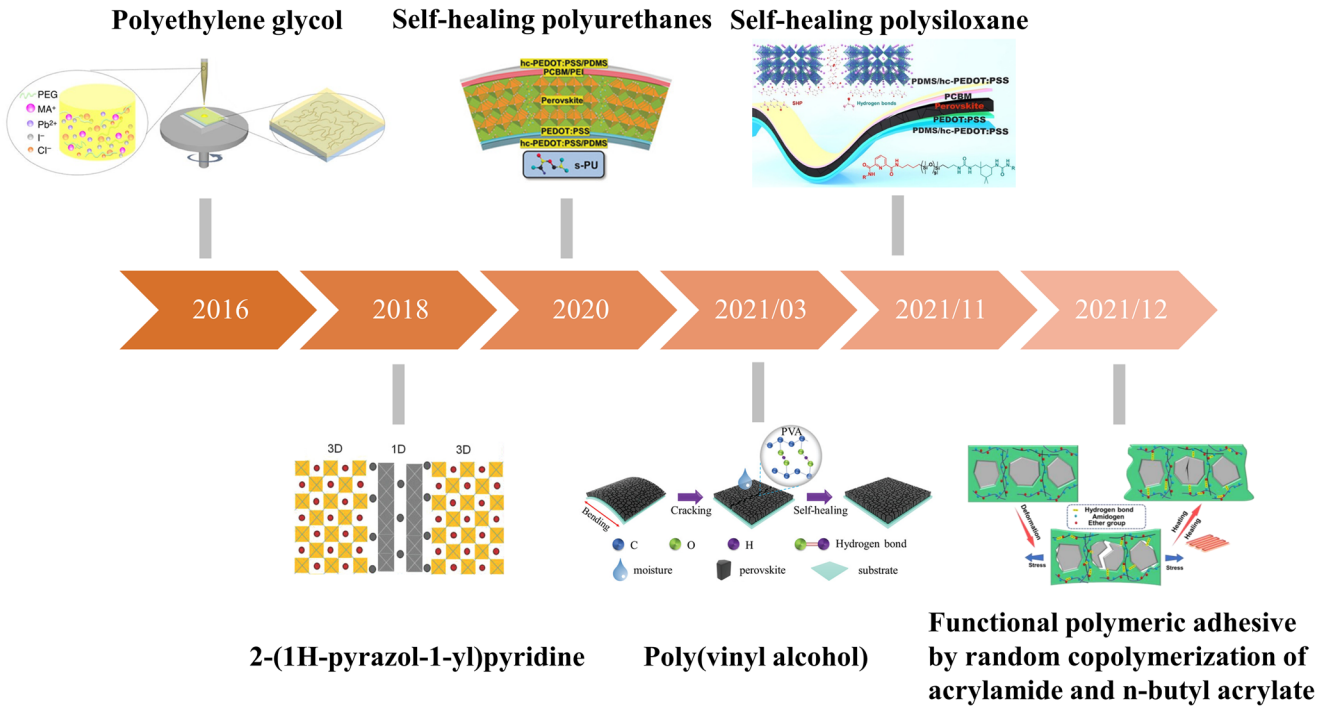


Figure 12. A timeline of representative works on self-healing PSCs and PPDs. Polyethylene glycol. Reproduced with permission.[130] Copyright 2016, Nature; 2-(1H-pyrazol-1-yl)pyridine). Reproduced with permission.[133] Copyright 2018, Wiley-VCH; Self-healing polyurethanes. Reproduced with permission.[134] Copyright 2020, Wiley-VCH; Poly(vinyl alcohol). Reproduced with permission.[135] Copyright 2021, Wiley-VCH; Self-healing polysiloxane. Reproduced with permission.[136] Copyright 2022, Wiley-VCH; Functional polymeric adhesive by random copolymerization of acrylamide and *n*-butyl acrylate. Reproduced with permission.[137] Copyright 2022, Wiley-VCH.

water, and so on, and when flexible perovskite devices are tested for flexibility, the fracture of the perovskite layer also greatly affects the performance of the device.

To solve the problem of the instability of perovskites, methods such as additive engineering, surface and interface passivation, and device encapsulation are used, which mainly play a role in delaying the decomposition of perovskites. Inspired by the natural self-healing ability of tissue and skin that can be restored to their original states without sacrificing function, scientists have begun to study the self-healing properties of perovskites to further expand the application of perovskite optoelectronic devices. Self-healing of perovskite refers to the use of some means to restore the original state after the perovskite material is destroyed. **Figure 12** depicts a timeline of representative works on self-healing perovskite devices, and the focus of these works is mainly on the self-healing perovskite layer. These methods include i) incorporating functional additive and ii) specific triggering conditions.

4.1. Incorporating Functional Additive

In this case, self-healing devices refer to the introduction of functional materials into the perovskite layer to activate self-healing effect. Mostly, self-healing polymers are added to perovskite precursor solutions. Benefiting from the special functional groups or polymer chains, a special force is formed between the polymer and perovskite materials to resist the erosion of water, and the underlying healing mechanism is based on the reversible weak chemical bonds formed in the polymer chains, such as hydrogen bonds, hydrophobic interactions, and dynamic covalent bonds.[127–129] Another type is to take advantage of the good moisture-proof and anti-oxidation properties of polymer materials to make them as encapsulation materials to resist external forces, thereby enhancing the stability of PSCs.[20]

Perovskite has a chemical formula of ABX_3, where A is a monovalent cation (e.g., methylammonium, formammidinium, or Cs), B is a divalent rare metal (Pb or Sn), and X is a halide anion (I, Br, or Cl).[11–13] Perovskite usually deposits AX and BX_2 into ABX_3 according to a certain stoichiometric ratio by the solution method, gas phase method, etc. When perovskite is decomposed by external factors such as heat, humidity, ultraviolet radiation, etc., the decomposition products are generally AX and BX_2 components. Therefore, by recombining the decomposed products AX and BX_2 to form ABX_3, the goal of self-healing is achieved. For example, Zhao's group prepared a polymer (polyethylene glycol) (PEG) scaffold perovskite layer at 105 °C in a one-step process (**Figure 13**a).[130] The presence of the PEG polymer greatly improved the moisture stability of the films and devices. The hygroscopicity of PEG materials can stabilize PSCs in a humid environment (Figure 13b). More importantly, the PEG-treated perovskite film exhibited a strong self-healing ability under steam spray. The test results showed that the PEG-containing perovskite film was sprayed with water vapor for 60 s and then gradually decomposed to form a yellow substance. After that, the water was removed by heating. After heating for 30 s, the yellow substance gradually

© 2022 Wiley-VCH GmbH

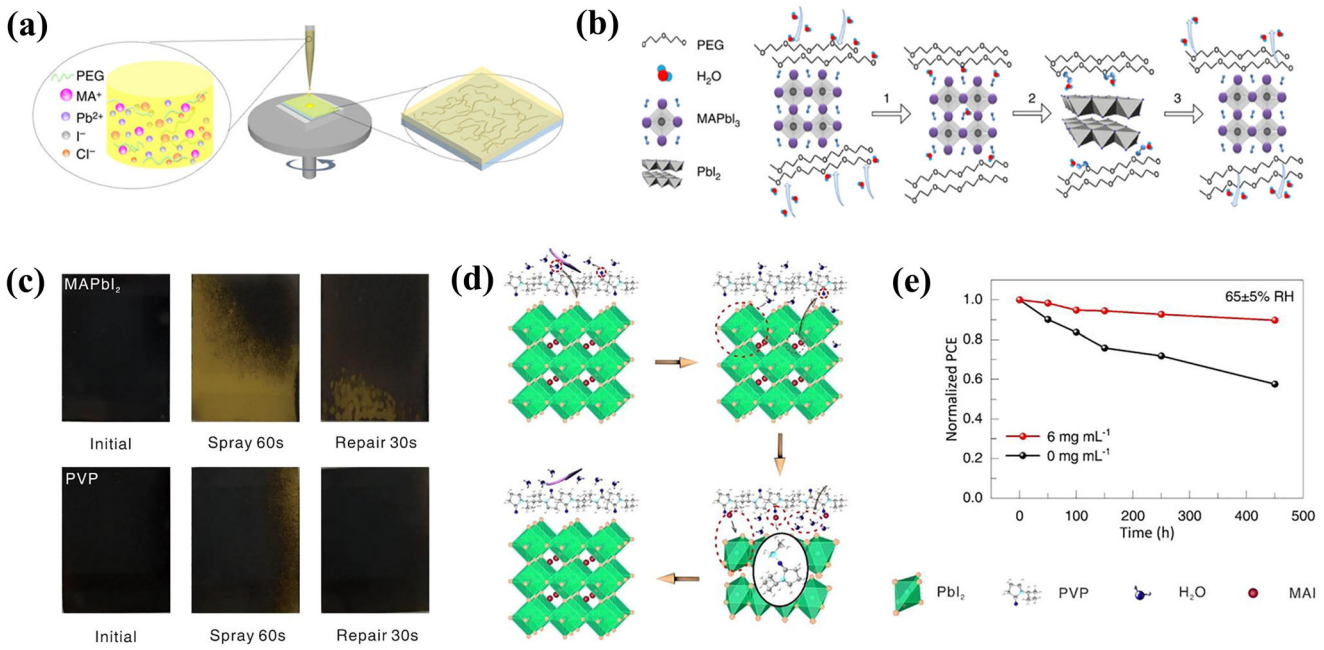


Figure 13. a) Schematic illustration of the fabrication of perovskite films with polymer scaffolds using a one-step spin coating method. b) Schematic illustration of the mechanism by which PEG repairs $MAPbI_3$. Reproduced with permission.[130] Copyright 2016, Nature. c) Changes in the color of films with and without PVP after 60 s of water spray and 30 s of self-healing. d) Schematic diagram of the self-healing process of perovskite thin films. e) Humidity stability of perovskite solar cells without and with PVP at 65% ± 5% RH humidity. Reproduced with permission.[132] Copyright 2022, ELSEVIER B.V. and Science Press.

disappeared. After further heating for 45 s, the yellow substance disappeared completely. This demonstrated the self-healing process of the perovskite film. Moreover, the *J–V* curve (performance is close to the initial value) and XRD (the disappearance of the PbI_2 peak) also proved this self-healing process. The yellow substance in the perovskite film without PEG did not disappear. This comparison showed that PEG played a key role in the self-healing process of perovskite. The reason why PEG works is that the OH^- in PEG and the I in perovskite form a bond to anchor PEG to the surfaces of perovskite grains. Due to the presence of water, the perovskite decomposes into PbI_2 and MAI, and MAI is anchored by PEG so as not to escape. When the water is evaporated, the decomposed PbI_2 and MAI recombine to form perovskite. This proves the commercial value of inexpensive, long-chain, and hygroscopic polymer scaffolds in PSCs. Inspired by the above work, Meng's group used PS as an additive to achieve a self-healing effect.[131] Recently, Hu's group achieved self-healing by adding PVP to perovskites.[132] The C=O···H—N hydrogen bond interaction at the grain boundary inhibited the decomposition of MA^+, improved the cyclic dissolution-recrystallization of perovskite, and finally achieved the self-healing phenomenon. After exposure, the original film quickly decomposed into PbI_2, and the film turned yellow, indicating that the perovskite was seriously damaged by water. In the optimized sample, the color of the perovskite with PVP basically remains unchanged, which is mainly because PVP more easily bonds with water molecules, preventing direct contact between the perovskite and water molecules. The films modified with PVP quickly returned to their original states after 30 s (Figure 13c). This is because there is a hydrogen bond interaction between PVP and MAI, so the MAI molecule can be fixed to prevent MAI from falling off or dissociating. (Figure 13d). After 500 h, the PCE of the PVP-modified battery was still above 90% (at 65% ± 5% RH), which was much higher than that of the control device (Figure 13e).

In addition to polymers, 1D materials can also achieve self-healing effects. Compared with 3D perovskites, 1D perovskites may have stronger thermodynamic stability due to their unique 1D structure. Mai's group incorporated 2-(1H-pyrazol-1-yl) pyridine (PZPY) into perovskite to obtain a series of 1D and/or 1D-3D Pb halide mixed perovskite materials.[133] Under the test conditions of 55% humidity and temperature cycling treatment (25–85 °C), the efficiency of the original sample dropped quickly, while the device processed by PZPY at the beginning of each temperature cycle had a certain level of recovery (**Figure 14**a,b). Moreover, as the concentration of PZPY additive increased, the self-healing ability of the 1D-3D PSCs was not as obvious. This is because when the concentration of PZPY is too high, it will adversely affect the PCE of the device. 1D PZPY played a key role in this PCE recovery process. Excessive heat can cause A^+ groups to detach from the perovskite lattice, which will lead to lattice vacancy defects and is not conducive to the stability of thin films and devices. However, small PZPY/PZPY-FAI cations are more flexible. PZPY is added to perovskite to form 1D perovskite, which blocks the migration of A^+, thus helping to inhibit the decomposition of 3D perovskite. In addition, the inherent properties of thermodynamically stable but kinetically movable 1D materials allow the system to repair lattice mismatches and passivate defects in the 1D–3D mixed perovskite heterojunction region that may occur during crystal growth. This is the reason for the self-repairing ability of the1D–3D PSC with temperature

© 2022 Wiley-VCH GmbH

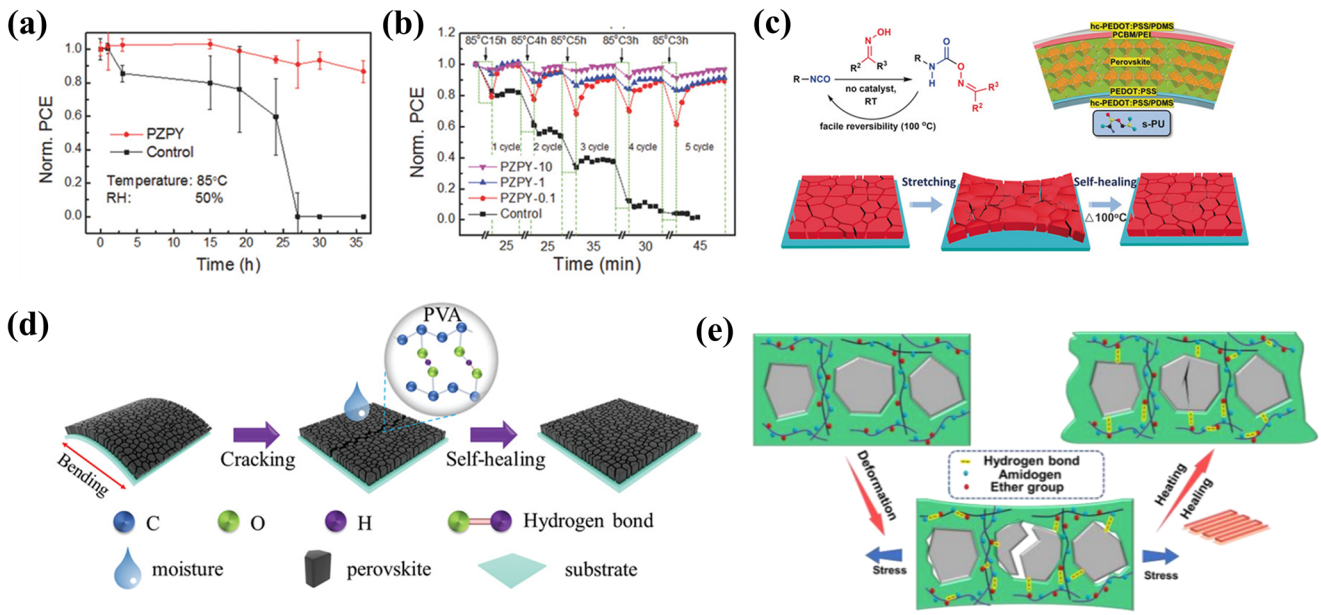


Figure 14. a) The thermal stability of PSCs without and with PZPY was maintained at 85 °C and 55% relative humidity (RH). b) Long-term stability of PSCs without and with PZPY during 55% RH temperature cycling (25–85 °C). Reproduced with permission.[133] Copyright 2018, Wiley-VCH. c) Schematic illustration of the stretchability and mechanical self-healing of PSCs. Reproduced with permission.[134] Copyright 2020, Wiley-VCH. d) Mechanisms of the self-healing process of perovskites with PVA. Reproduced with permission.[135] Copyright 2021, Wiley-VCH. e) *J–V* test of the thermally induced self-healing experiment. Reproduced with permission.[137] Copyright 2022, Wiley-VCH.

cycling. During the self-healing process, the structural phase transition between PbX_2-PZPY and PbX_2-FAI-PZPY can rebuild and strengthen the 3D lattice structure. This work will provide new research ideas for the design of low-dimensional perovskite active materials and devices under development, and these designs will lay the foundation for improving the long-term stability of perovskite-based optoelectronic devices.

Aside from the decomposition of perovskite materials due to the influence of external environmental factors, mechanical stress may also cause fracture at the grain boundaries, causing the performance of perovskites devices to decline. This is mainly due to the large number of defects at the perovskite grain boundaries. The water and oxygen in the air will also destroy the perovskite preferentially from the grain boundaries, and the existence of cracks is not conducive to the transport of carriers. The method for improving the mechanical stability of the perovskite film was introduced in the previous chapter on flexible devices. In this section, the method for repairing mechanical damage is mainly introduced. Self-healing materials usually have chemical bonds, such as hydrogen bonds, which can be rebuilt to repair the cracks when they break, thereby restoring the integrity of the perovskite film and allowing the device to continue working. Chen's group introduced self-healing polyurethanes (s-PU) with a dynamic covalent oxime-carbamate structure as a scaffold in the process of perovskite crystallization.[134] The presence of s-PU not only enhanced the flexibility of films and devices but also played a role in self-healing after annealing (Figure 14c). The test results showed that the hydrophobic s-PU elastomer completely filled the grain boundaries, which allowed s-PU-PSCs to maintain an initial efficiency of 86% after 3000 h under 1 sun illumination under atmospheric conditions. More importantly, due to dynamic oxime—carbamate bonds, s-PU can effectively repair cracks caused by grain boundary stretching through a simple thermodynamic self-healing process. After 1000 cycles, the final device can recover more than 90% of the original PCE under 20% tensile stress. Our group designed a water-triggered self-healing flexible PPD containing poly(vinyl alcohol) (PVA) as an additive (Figure 14d).[135] By adding PVA directly into the perovskite precursor solution, the double functions of self-healing and flexibility are realized. When cracks appeared at the perovskite grain boundaries after bending, PVA activated the hydroxyl group under 80% humidity, leading to self-healing in a relatively short amount of time. After 1000 bending cycles, the performance of the PVA-$FAPbI_3$ and $FAPbI_3$ devices decreased to ≈75% and 40% of the initial values, respectively. After being placed in a dry environment for 12 h, the performances of the two devices were almost unchanged. Finally, when placed in an environment with a humidity of 80% for a period of time, the $FAPbI_3$ device quickly degraded within 5 h, while the PVA-$FAPbI_3$ device recovered more than 90% of the initial performance after 8–9 h of storage, showing an outstanding self-healing ability. This is due to the H bonds in PVA repairing the cracks of the perovskite with the assistance of water molecules. It is worth noting that PVA does not negatively affect the transport of carriers, and this self-healing process can be repeated for five cycles. This method of repairing damage to perovskite films caused by mechanical forces is very suitable for application in the preparation of stable flexible wearable optoelectronic devices. Huang's group used a self-healing polysiloxane (SHP) to achieve self-healing.[136] During the bending process, the SHP at the grain boundary was preferentially fractured to relieve the bending stress. Without annealing treatment, the abundant hydrogen bonds of SHP can enable the self-healing of grain boundary cracks in the film. Recently, Dong's group used a supramolecular adhesive that can

© 2022 Wiley-VCH GmbH

repair cracks created by bending the film (Figure 14e).[137] Experimental studies on repairing cracks are beneficial to promote the further development of flexible devices.

4.2. Specific Triggering Conditions

The performance of perovskite devices degrades after a long period of light irradiation, and some reports attribute it to the effect of UV light on the active layer or ion migration.[138] PSCs or PPDs inevitably suffer from short-circuit current (J_{SC}) or photocurrent (I_P) losses under continuous illumination, while Nie's group found that when the device was left in the dark state for a period of time, J_{SC} or I_P would return to the initial state.[139] The results showed that whether it was open-circuit or short-circuit, under 1 sun illumination, the V_{OC} of the device basically did not change after reaching a stable value, and when the light continued, J_{SC} would drop. This slow decay was due to the formation of photoactivated metastable deep-level trap states. After stabilizing for a period of time in the dark state, J_{SC} will return to its initial value. PCE also conformed to this law of change. The measurement showed that excessive exposure of the device to light will lead to a current drop. Under constant 1 sun illumination, there were an increasing number of photoactive elements in a stable state, which accumulated within tens of minutes to several hours, causing most of the film to form a charged area, which in turn led to photocurrent degradation (photodegradation state). However, when the device was resting in the dark, most of these light-activated trap states disappeared. When the light continued, the photocurrent (and PCE) recovered to close to 100% of its initial steady-state value (self-healing state). In addition, external proton radiation can also achieve self-healing of PSCs. Lang's group prepared inverted PSCs and irradiated the devices with 68 MeV protons. When the proton irradiation was terminated, the perovskite's self-healing process began and the J_{SC} recovered. After 10 days, V_{OC} and fill factor were significantly enhanced compared to the reference device. Radiation-induced damage led to dissociation of C—H and N—H bonds, resulting in the formation of localized defect states that act as recombination centers in the band gap. Then, the displaced hydrogen atoms migrated in the perovskite lattice and passivated the local defects.[140] Compared with polycrystalline perovskite films, single crystal materials have better carrier diffusion lengths, carrier lifetimes, and defect density of states. However, perovskite single crystals are brittle and fragile, which limits their application in optoelectronic devices. More recently, Naumov's group achieved autonomous self-healing of $MAPbI_3$ single crystal materials with minimal compression at ambient temperature, taking advantage of the high ionic mobility, low binding energy, dynamic structural defects, soft crystalline lattice, and other properties of $MAPbI_3$ materials.[141] They separated the $MAPbI_3$ single crystal into halves using a blade perpendicular to the (100) plane but parallel to the (001) plane of the single crystal and then applied a minimum force (0.65–1.5 N) to ensure contact between the fractured interfaces under nitrogen for 24 h. The results showed that the fracture surface healed and reassembled into a whole. By fabricating it into optoelectronic devices and testing the *I–V* curves, the photocurrent of the device based on the healed single-crystal material recovered to 74% of the original value, indicating that a large amount of photocurrent can still be generated in the crystal after healing. These results show that $MAPbI_3$ can still achieve self-healing after mechanical damage without additives. The studies on self-healing PSCs and PPDs mentioned in this section are summarized in **Table 3**.

In summary, the self-healing PSCs and PPDs have achieved exciting results in promoting device lifespan and long-term stability. However, the research on self-healing perovskite device is still in its infancy, and many basic works need to be carried out. The following aspects should be paid more attention to in future research: i) Since the incorporation of self-healing additives would influence the fabrication window of the PSCs and PPDs, it is crucial to develop compatible and universal self-healing materials to broaden the working window. ii) Considering the self-healing polymeric materials are almost ionically and electrically insulating, it is desired to fabricate self-healing additives with intrinsic conductivity so as to benefit the charge transfer properties. iii) Currently, the understanding of the self-healing mechanism is too shallow. To gain insight into the underlying mechanism of self-healing PSCs and PPDs, it is necessary to develop and utilize in situ characterization techniques and molecular simulation.

5. Conclusion and Outlook

This review mainly summarizes the three functional directions of perovskite PSCs/PPDs, that is, flexibility, transparency, and self-healing. Flexible PPDs/PSCs require their components, including the substrate, electrode, and perovskite, to have good flexibility. For flexible substrates, electrodes and perovskites, there are many options. Among them, the most widely used substrates are polymers. However, polymer substrates have the disadvantages of high cost and low temperature resistance, so other alternative options have been developed. Electrodes and perovskites are important components of optoelectronic devices. There are many materials and methods to choose from to fabricate flexible devices. Finally, methods for achieving flexible perovskite devices are introduced from the viewpoint of different perovskite structures.

Semitransparent devices require all components, including electrodes and perovskite layers, to have semitransparent characteristics. The commonly used substrate material is glass. Even opaque devices require a highly transparent substrate to transmit enough light to allow the perovskite layer to absorb light, so the substrate itself has high transparency. An effective and feasible way to reduce its light absorption amount and light absorption range is to make the perovskite layer have a certain light transmittance. This article introduces the realization of semitransparent perovskite through the following three methods: i) reduce the perovskite coverage, ii) decrease the perovskite thickness, and iii) adjust the band gap of perovskite. For i) and ii), translucency is achieved mainly by reducing the amount of light absorption of the perovskite in the light absorption range. For iii), translucency is achieved mainly by reducing the light absorption range of the perovskite. In addition to the perovskite layer, the traditional opaque electrode layer is also a problem to be solved. The researchers introduced transparent metal oxides, thin metals, metal NWs and other materials with high transparency and good conductivity as substrates.

Self-healing PSCs and PPDs mainly achieve the function of self-healing through the self-repair of perovskite. Self-repairing

© 2022 Wiley-VCH GmbH

Table 3. The mechanism and advantages of different self-healing materials.

	Materials	Mechanism	Advantages
Self-healing PSCs/PPDs (Perovskite)	PEG, PS, PVP, 1D PZPY	Binds to the perovskite component AX or BX_2 to prevent its volatilization and promotes the recombination of AX and BX_2 into ABX_3	Improve device wet stability
	s-PU, PVA, SHP	Under the stimulation of external conditions (water, heat, light), self-healing materials play a role in repairing cracks and achieving self-healing	Improve device mechanical stability
	Specific conditions	Self-healing in the dark	No additives required

optoelectronic devices have a longer service life than traditional optoelectronic devices, which is beneficial in practical applications. This article introduces two situations in which degraded perovskite and cracked perovskite are restored to their initial states, which helps to improve the long-term stability and flexibility of the devices. At the same time, the device can be restored to its initial state by allowing it to rest in a dark state for a period of time after being exposed to light for a long time. In short, repairing damaged perovskites to restore their photoelectric performance to the original state is one of the development directions for perovskite photovoltaic devices.

However, it is undeniable that compared with traditional rigid and opaque devices, flexible and semitransparent devices have more stringent conditions for the selection of the materials of each component, which will increase production costs. Therefore, to balance performance and cost, researchers need to do much work. For example, low-cost materials and additives, component engineering, interface optimization, etc., can be used to improve device performance. While achieving flexibility and translucency, part of the performance of the device will inevitably be sacrificed, especially for semitransparent devices. Insufficient light absorption leads to a reduction in current. In general, implementing functionality inevitably requires some performance to be sacrificed. Balancing the relationship between the two is the focus of future research. The realization of self-healing photovoltaic devices greatly improves the service life of the devices and reduces the loss of materials, which is in line with the concept of green, energy-saving, and sustainable development.

At present, the performance of PPDs and PSCs has reached a very high level. To achieve their application in practice, it is necessary to functionalize them by developing flexible, semitransparent, and self-healing devices. In this process, the following should be pursued: i) improved performance; ii) cost control; and iii) realizing two or more functions at the same time. Performance is the basis of its practical application. The cost makes it possible to use it on a large scale. The combination of flexibility and self-healing or semitransparent characteristics can greatly increase the service life and application of the devices. For example, a flexible device will break during the bending process. After combining with a self-healing material containing a large number of hydrogen bonds, the break will be repaired, which will greatly extend the service life of the flexible device. In addition, an important way to realize a semitransparent device is to reduce the thickness of the material to increase the light transmittance, and reducing the thickness of the material is very helpful to improve its softness, which means that translucency and flexibility have certain compatibility. Furthermore, the unevenly distributed perovskite layer facilitates the realization of translucency. However, these artificial voids will increase the risk of perovskite being eroded by water and oxygen. When combined with self-healing materials (such as PEG, PVP, PS, etc.), the components can be reconstructed after decomposition, which will greatly increase the life of the perovskite and the devices. This is one of the basic conditions for the practical application of optoelectronic devices. In summary, the functionalization of PSCs and PPDs is an inevitable trend of their development, and how to better realize functionalization is a research focus in the future. If two or more functionalizations can be realized at the same time, it will greatly increase the commercial competitiveness of the devices. Although the strategies for realizing these three functionalizations determine that the three functions have certain compatibility, there are few studies on realizing two or more functions at the same time.[142–144] We hope this review can provide new ideas for future research.

Another important factor affecting the practical application of perovskite devices is that they contain Pb, which is toxic. The solution is to replace Pb with other nontoxic or low-toxic elements (Sn, Ge, Bi, etc.). However, perovskites based on these elements usually suffer from the disadvantages of being easily oxidized, being expensive, and having poor film formation. More importantly, compared with lead-based devices, devices based on these lead-free perovskites have lower performance and cannot meet actual needs. Therefore, it is feasible to improve the performance and stability of lead-free perovskite optoelectronic devices. In the process of commercialization of perovskite optoelectronic devices, the service life is a point of great concern, which is closely related to the stability of perovskite. Improving the stability of perovskite devices has always been a research focus of researchers. The measures taken include additive engineering, surface passivation, packaging, etc., which have been quite effective, but the cost is high. Therefore, it is still necessary to consider methods with universal low cost. We believe that with the efforts of researchers, the commercialization of perovskite optoelectronic devices is just around the corner and will bring great convenience to people's lives.

Acknowledgements

The authors acknowledge the support from the National Natural Science Foundation of China (Nos. 52025028, 52072254, 51872191, 12074277), the Innovative Science and Technology Platform Project of Cooperation between Yangzhou City and Yangzhou University, China (No.

 © 2022 Wiley-VCH GmbH

YZ2020263), the Key University Science Research Project of Jiangsu Province (21KJA430005), the fund of the State Key Laboratory of Solidification Processing in NPU (Grant No. SKLSP202219), and the Priority Academic Program Development of Jiangsu Higher Education Institutions.

Conflict of Interest

The authors declare no conflict of interest.

Keywords

flexible, perovskite solar cells, photodetectors, self-healing, semitransparent

Received: August 23, 2022
Revised: October 26, 2022
Published online: December 27, 2022

[1] Q. Tai, K. Tang, F. Yan, *Energy Environ. Sci.* **2019**, *12*, 2375.
[2] Y. B. Cheng, A. Pascoe, F. Huang, Y. Peng, *Nature* **2016**, *539*, 488.
[3] M. H. Kumar, N. Yantara, S. Dharani, M. Graetzel, S. Mhaisalkar, P. P. Boix, N. Mathews, *Chem. Commun.* **2013**, *49*, 11089.
[4] G. Konstantatos, G. Konstantatos, I. Howard, A. Fischer, S. Hoogland, J. Clifford, E. Klem, L. Levina, E. H. Sargent, *Nature* **2006**, *442*, 180.
[5] D. Palaferri, Y. Todorov, A. Bigioli, A. Mottaghizadeh, D. Gacemi, A. Calabrese, A. Vasanelli, L. Li, A. G. Davies, E. H. Linfield, F. Kapsalidis, M. Beck, J. Faist, C. Sirtori, *Nature* **2018**, *556*, 85.
[6] X. Yu, Y. Li, X. Hu, D. Zhang, Y. Tao, Z. Liu, Y. He, M. A. Haque, Z. Liu, T. Wu, Q. J. Wang, *Nat. Commun.* **2018**, *9*, 4299.
[7] Best Research-Cell Efficiency Chart, **2022**. https://www.nrel.gov/pv/cell-efficiency.html.
[8] Y. Guan, C. Zhang, Z. Liu, Y. Zhao, A. Ren, J. Liang, F. Hu, Y. S. Zhao, *Adv. Mater.* **2022**, *34*, 2203201.
[9] D. Wu, W. Li, H. Liu, X. Xiao, K. Shi, H. Tang, C. Shan, K. Wang, X. W. Sun, A. K. K. Kyaw, *Adv. Sci.* **2021**, *8*, 2101729.
[10] M. Razeghi, A. Rogalski, *J. Appl. Phys.* **1996**, *79*, 7433.
[11] M. Sessolo, L. Gil-Escrig, G. Longo, H. J. Bolink, *Top. Curr. Chem.* **2016**, *374*, 52.
[12] A. Jodlowski, D. Rodríguez-Padrón, R. Luque, G. Miguel, *Adv. Energy Mater.* **2018**, *8*, 1703120.
[13] T. He, Y. Jiang, X. Xing, M. Yuan, *Adv. Mater.* **2020**, *32*, 1903937.
[14] Z. Liu, L. K. Ono, Y. Qi, *J. Energy Chem.* **2020**, *46*, 215.
[15] G. Tang, F. Yan, *Nano Today* **2021**, *39*, 101155.
[16] D. Hao, J. Zou, J. Huang, *InfoMat* **2019**, *2*, 139.
[17] P. You, Z. Liu, Q. Tai, S. Liu, F. Yan, *Adv. Mater.* **2015**, *27*, 3632.
[18] F. R. Li, Y. Xu, W. Chen, S. H. Xie, J. Y. Li, *J. Mater. Chem. A* **2017**, *5*, 10374.
[19] H. Liu, H. Zhou, *Chem. Res. Chin. Univ.* **2021**, *37*, 1055.
[20] Y. Yu, F. Zhang, H. Yu, *Sol. Energy* **2020**, *209*, 408.
[21] W. Tian, H. Zhou, L. Li, *Small* **2017**, *13*, 1702107.
[22] K. Qian, R. Y. Tay, M. F. Lin, J. Chen, H. Li, J. Lin, J. Wang, G. Cai, V. C. Nguyen, E. H. Teo, T. Chen, P. S. Lee, *ACS Nano* **2017**, *11*, 1712.
[23] X. Hu, X. Zhang, L. Liang, J. Bao, S. Li, W. Yang, Y. Xie, *Adv. Funct. Mater.* **2014**, *24*, 7373.
[24] F. Cao, W. Tian, L. Meng, M. Wang, L. G. Li, *Adv. Funct. Mater.* **2019**, *29*, 1906756.
[25] T. Vemulkar, R. Mansell, A. Fernández-Pacheco, R. P. Cowburn, *Adv. Funct. Mater.* **2016**, *26*, 4704.
[26] Y. Chen, C. Zhao, T. Zhang, X. Wu, W. Zhang, S. J. Ding, *Small* **2021**, *17*, 2007543.
[27] D. Li, W. Y. Lai, Y. Z. Zhang, W. Huang, *Adv. Mater.* **2018**, *30*, 1704738.
[28] M. Hassan, G. Abbas, N. Li, A. Afzal, Z. Haider, S. Ahmed, X. Xu, C. Pan, Z. Peng, *Adv. Mater. Technol.* **2021**, *7*, 2100773.
[29] H. S. Jung, G. S. Han, N. Park, M. J. Ko, *Joule* **2019**, *3*, 1850.
[30] J. Lee, J. Kim, T. Hyeon, *Adv. Mater.* **2006**, *18*, 2073.
[31] R. L. McCreery, *Chem. Rev.* **2008**, *108*, 2646.
[32] H. Sun, T. Lei, W. Tian, F. Cao, J. Xiong, L. Li, *Small* **2017**, *13*, 1701042.
[33] H. Sun, W. Tian, F. Cao, J. Xiong, L. Li, *Adv. Mater.* **2018**, *30*, 1706986.
[34] D. Tobjork, R. Osterbacka, *Adv. Mater.* **2011**, *23*, 1935.
[35] D. H. Lien, Z. K. Kao, T. H. Huang, Y. C. Liao, S. C. Lee, J. H. He, *ACS Nano* **2014**, *8*, 7613.
[36] J. L. Delaney, C. F. Hogan, J. Tian, W. Shen, *Anal. Chem.* **2011**, *83*, 1300.
[37] J. Liu, C. Yang, H. Wu, Z. Lin, Z. Zhang, R. Wang, B. Li, F. Kang, L. Shi, C. P. Wong, *Energy Environ. Sci.* **2014**, *7*, 3674.
[38] Y. H. Jung, T. H. Chang, H. Zhang, C. Yao, Q. Zheng, V. W. Yang, H. Mi, M. Kim, S. J. Cho, D. W. Park, H. Jiang, J. Lee, Y. Qiu, W. Zhou, Z. Cai, S. Gong, Z. Ma, *Nat. Commun.* **2015**, *6*, 7170.
[39] H. Fang, J. Li, J. Ding, Y. Sun, Q. Li, J. L. Sun, L. Wang, Q. Yan, *ACS Appl. Mater. Interfaces* **2017**, *9*, 10921.
[40] Y. He, H. Dong, Q. Meng, L. Jiang, W. Shao, L. He, W. Hu, *Adv. Mater.* **2011**, *23*, 5502.
[41] S. Ke, C. Chen, N. Fu, H. Zhou, M. Ye, P. Lin, W. Yuan, X. Zeng, L. Chen, H. Huang, *ACS Appl. Mater. Interfaces* **2016**, *8*, 28406.
[42] J. Jiang, Y. Bitla, C. W. Huang, T. H. Do, H. J. Liu, Y. H. Hsieh, C. H. Ma, C. Y. Jang, Y. H. Lai, P. W. Chiu, W. W. Wu, Y. C. Chen, Y. C. Zhou, Y. H. Chu, *Sci. Adv.* **2017**, *3*, 1700121.
[43] T. Amrillah, Y. Bitla, K. Shin, T. Yang, Y. H. Hsieh, Y. Y. Chiou, H. J. Liu, T. H. Do, D. Su, Y. C. Chen, S. U. Jen, L. Q. Chen, K. H. Kim, J. Y. Juang, Y. H. Chu, *ACS Nano* **2017**, *11*, 6122.
[44] C. Jia, X. Zhao, Y. Lai, J. Zhao, P. Wang, D. Liou, P. Wang, Z. Liu, W. Zhang, W. Chen, Y. Chu, J. Li, *Nano Energy* **2019**, *60*, 476.
[45] S. K. Balasingam, M. G. Kang, Y. Jun, *Chem. Commun.* **2013**, *49*, 11457.
[46] G. E. Eperon, V. M. Burlakov, A. Goriely, H. J. Snaith, *ACS Nano* **2014**, *8*, 591.
[47] L. Zuo, C. C. Chueh, Y. X. Xu, K. S. Chen, Y. Zang, C. Z. Li, H. Chen, A. K. Jen, *Adv. Mater.* **2014**, *26*, 6778.
[48] M. Lee, Y. Jo, D. S. Kim, Y. Jun, *J. Mater. Chem. A* **2015**, *3*, 4129.
[49] M. Junghähnel, S. Garner, *Vak. Forsch. Prax.* **2014**, *26*, 35.
[50] W. L. Rance, J. M. Burst, D. M. Meysing, C. A. Wolden, M. O. Reese, T. A. Gessert, W. K. Metzger, S. Garner, P. Cimo, T. M. Barnes, *Appl. Phys. Lett.* **2014**, *104*, 143903.
[51] M. M. Tavakoli, K. H. Tsui, Q. Zhang, J. He, Y. Yao, D. Li, Z. Fan, *ACS Nano* **2015**, *9*, 10287.
[52] X. Dai, Y. Deng, C. H. V. Brackle, S. Chen, P. N. Rudd, X. Xiao, Y. Lin, B. Chen, J. Huang, *Adv. Energy Mater.* **2019**, *10*, 1903108.
[53] M. Yousaf, H. Tian, H. Shi, Y. Wang, Y. Chen, Z. Ma, A. Cao, H. E. Naguib, R. P. S. Han, *Adv. Energy Mater.* **2016**, *6*, 1600490.
[54] K. G. Lim, T. H. Han, T. W. Lee, *Energy Environ. Sci.* **2021**, *14*, 2009.
[55] Z. Liu, S. P. Lau, F. Yan, *Chem. Soc. Rev.* **2015**, *44*, 5638.
[56] Z. Yin, J. Zhu, Q. He, X. Cao, C. Tan, H. Chen, Q. Yan, H. Zhang, *Adv. Energy Mater.* **2014**, *4*, 1300574.
[57] J. Du, S. Pei, L. Ma, H. M. Cheng, *Adv. Mater.* **2014**, *26*, 1958.
[58] Z. Liu, P. You, C. Xie, G. Tang, F. Yan, *Nano Energy* **2016**, *28*, 151.
[59] Q. Luo, H. Ma, Q. Hou, Y. Li, J. Ren, X. Dai, Z. Yao, Y. Zhou, L. Xiang, H. Du, H. He, N. Wang, K. Jiang, H. Lin, H. Zhang, Z. Guo, *Adv. Funct. Mater.* **2018**, *28*, 1706777.
[60] S. Ye, A. R. Rathmell, Z. Chen, I. E. Stewart, B. J. Wiley, *Adv. Mater.* **2014**, *26*, 6670.
[61] R. A. Hatton, M. R. Willis, M. A. Chesters, D. Briggs, *J. Mater. Chem.* **2003**, *13*, 722.

 © 2022 Wiley-VCH GmbH

[62] N. Formica, D. S. Ghosh, T. L. Chen, C. Eickhoff, I. Bruder, V. Pruneri, *Sol. Energy Mater. Sol. Cells* **2012**, *107*, 63.
[63] T. B. Song, Y. S. Rim, F. Liu, B. Bob, S. Ye, Y. T. Hsieh, Y. Yang, *ACS Appl. Mater. Interfaces* **2015**, *7*, 24601.
[64] H. Lee, S. Hong, J. Lee, Y. D. Suh, J. Kwon, H. Moon, H. Kim, J. Yeo, S. H. Ko, *ACS Appl. Mater. Interfaces* **2016**, *8*, 15449.
[65] X. Dai, Y. Zhang, H. Shen, Q. Luo, X. Zhao, J. Li, H. Lin, *ACS Appl. Mater. Interfaces* **2016**, *8*, 4523.
[66] A. Kim, H. Lee, H. C. Kwon, H. S. Jung, N. G. Park, S. Jeong, J. Moon, *Nanoscale* **2016**, *8*, 6308.
[67] E. Lee, J. Ahn, H.-C. Kwon, S. Ma, K. Kim, S. Yun, J. Moon, *Adv. Energy Mater.* **2018**, *8*, 1702182.
[68] G. Jeong, D. Koo, J. Seo, S. Jung, Y. Choi, J. Lee, H. Park, *Nano Lett.* **2020**, *20*, 3718.
[69] M. Li, W. W. Zuo, A. G. Ricciardulli, Y. G. Yang, Y. H. Liu, Q. Wang, K. L. Wang, G. X. Li, M. Saliba, D. Di Girolamo, A. Abate, Z. K. Wang, *Adv. Mater.* **2020**, *32*, 2003422.
[70] F. Yang, J. Liu, Z. Lu, P. Dai, T. Nakamura, S. Wang, L. Chen, A. Wakamiya, K. Matsuda, *Adv. Sci.* **2020**, *7*, 1902474.
[71] G. Cen, Y. Liu, C. Zhao, G. Wang, Y. Fu, G. Yan, Y. Yuan, C. Su, Z. Zhao, W. Mai, *Small* **2019**, *15*, 1902135.
[72] Y. Liu, J. Sun, Z. Yang, D. Yang, X. Ren, H. Xu, Z. Yang, S. F. Liu, *Adv. Opt. Mater.* **2016**, *4*, 1829.
[73] Y. Bai, H. Zhang, M. Zhang, D. Wang, H. Zeng, J. Zhao, H. Xue, G. Wu, J. Su, Y. Xie, Y. Zhang, H. Jing, H. Yu, Z. Hu, R. Peng, M. Wang, Y. Wu, *Nanoscale* **2020**, *12*, 1100.
[74] D. Shi, V. Adinolfi, R. Comin, M. Yuan, E. Alarousu, A. Buin, Y. Chen, S. Hoogland, A. Rothenberger, K. Katsiev, Y. Losovyj, X. Zhang, P. A. Dowben, O. F. Mohammed, E. H. Sargent, O. M. Bakr, *Science* **2015**, *347*, 519.
[75] M. I. Saidaminov, A. L. Abdelhady, B. Murali, E. Alarousu, V. M. Burlakov, W. Peng, I. Dursun, L. Wang, Y. He, G. Maculan, A. Goriely, T. Wu, O. F. Mohammed, O. M. Bakr, *Nat. Commun.* **2015**, *6*, 7586.
[76] Q. Dong, Y. Fang, Y. Shao, P. Mulligan, J. Qiu, L. Cao, J. Huang, *Science* **2015**, *347*, 967.
[77] Y. Liu, Y. Zhang, Z. Yang, H. Ye, J. Feng, Z. Xu, X. Zhang, R. Munir, J. Liu, P. Zuo, Q. Li, M. Hu, L. Meng, K. Wang, D. M. Smilgies, G. Zhao, H. Xu, Z. Yang, A. Amassian, J. Li, K. Zhao, S. F. Liu, *Nat. Commun.* **2018**, *9*, 5302.
[78] H. Jing, R. Peng, R. M. Ma, J. He, Y. Zhou, Z. Yang, C. Y. Li, Y. Liu, X. Guo, Y. Zhu, D. Wang, J. Su, C. Sun, W. Bao, M. Wang, *Nano Lett.* **2020**, *20*, 7144.
[79] R. Ding, Y. Lyu, Z. Wu, F. Guo, W. F. Io, S. Y. Pang, Y. Zhao, J. Mao, M. C. Wong, J. Hao, *Adv. Mater.* **2021**, *33*, 2101263.
[80] C. Bi, B. Chen, H. Wei, S. DeLuca, J. Huang, *Adv. Mater.* **2017**, *29*, 1605900.
[81] M. Li, Y. G. Yang, Z. K. Wang, T. Kang, Q. Wang, S. H. Turren-Cruz, X. Y. Gao, C. S. Hsu, L. S. Liao, A. Abate, *Adv. Mater.* **2019**, *31*, 1901519.
[82] Z. Saki, M. M. Byranvand, N. Taghavinia, M. Kedia, M. Saliba, *Energy Environ. Sci.* **2021**, *14*, 5690.
[83] W. Deng, F. Li, J. Li, M. Wang, Y. Hu, M. Liu, *Nano Energy* **2020**, *70*, 104505.
[84] S. Sanchez, X. Hua, P. Nga, U. Steiner, A. Abate, *Adv. Energy Mater.* **2018**, *8*, 1702915.
[85] C. C. Zhang, S. Yuan, Y. H. Lou, Q. W. Liu, M. Li, H. Okada, Z. K. Wang, *Adv. Mater.* **2020**, *32*, 2001479.
[86] X. Meng, Z. Cai, Y. Zhang, X. Hu, Z. Xing, Z. Huang, Z. Huang, Y. Cui, T. Hu, M. Su, X. Liao, L. Zhang, F. Wang, Y. Song, Y. Chen, *Nat. Commun.* **2020**, *11*, 3016.
[87] Q. Dong, M. Chen, Y. Liu, F. T. Eickemeyer, W. Zhao, Z. Dai, Y. Yin, C. Jiang, J. Feng, S. Jin, S. Liu, S. M. Zakeeruddin, M. Grätzel, N. P. Padture, Y. Shi, *Joule* **2021**, *5*, 1587.
[88] W. Tian, L. Min, F. Cao, L. Li, *Adv. Mater.* **2020**, *32*, 1906974.
[89] H. Chen, H. Wang, J. Wu, F. Wang, T. Zhang, Y. Wang, D. Liu, S. Li, R. V. Penty, I. H. White, *Nano Res.* **2020**, *13*, 1997.
[90] K. Shen, H. Xu, X. Li, J. Guo, S. Sathasivam, M. Wang, A. Ren, K. L. Choy, I. P. Parkin, Z. Guo, J. Wu, *Adv. Mater.* **2020**, *32*, 2000004.
[91] L. Hu, Q. Zhao, S. Huang, J. Zheng, X. Guan, R. Patterson, J. Kim, L. Shi, C. H. Lin, Q. Lei, D. Chu, W. Tao, S. Cheong, R. D. Tilley, A. W. Y. Ho-Baillie, J. M. Luther, J. Yuan, T. Wu, *Nat. Commun.* **2021**, *12*, 466.
[92] J. B. Hoffman, A. L. Schleper, P. V. Kamat, *J. Am. Chem. Soc.* **2016**, *138*, 8603.
[93] Y. Zhou, J. Luo, Y. Zhao, C. Ge, C. Wang, L. Gao, C. Zhang, M. Hu, G. Niu, J. Tang, *Adv. Opt. Mater.* **2018**, *6*, 1800679.
[94] Q. Zhou, J. G. Park, R. Nie, A. K. Thokchom, D. Ha, J. Pan, S. I. Seok, T. Kim, *ACS Nano* **2018**, *12*, 8406.
[95] F. Cao, W. Tian, M. Wang, H. Cao, L. Li, *Adv. Funct. Mater.* **2019**, *29*, 1901280.
[96] M. Wang, W. Tian, F. Cao, M. Wang, L. Li, *Adv. Funct. Mater.* **2020**, *30*, 1909771.
[97] D. Wu, H. Zhou, Z. Song, M. Zheng, R. Liu, X. Pan, H. Wan, J. Zhang, H. Wang, X. Li, H. Zeng, *ACS Nano* **2020**, *14*, 2777.
[98] X. Li, D. Yu, J. Chen, Y. Wang, F. Cao, Y. Wei, Y. Wu, L. Wang, Y. Zhu, Z. Sun, J. Ji, Y. Shen, H. Sun, H. Zeng, *ACS Nano* **2017**, *11*, 2015.
[99] Z. Li, S. A. Kulkarni, P. P. Boix, E. Shi, A. Cao, K. Fu, S. K. Batabyal, J. Zhang, Q. Xiong, L. H. Wong, N. Mathews, S. G. Mhaisalkar, *ACS Nano* **2014**, *8*, 6797.
[100] Q. Xue, R. Xia, C. J. Brabec, H.-L. Yip, *Energy Environ. Sci.* **2018**, *11*, 1688.
[101] L. Mazzarella, Y.-H. Lin, S. Kirner, A. B. Morales-Vilches, L. Korte, S. Albrecht, E. Crossland, B. Stannowski, C. Case, H. J. Snaith, R. Schlatmann, *Adv. Energy Mater.* **2019**, *9*, 1803241.
[102] F. Sahli, J. Werner, B. A. Kamino, M. Brauninger, R. Monnard, B. Paviet-Salomon, L. Barraud, L. Ding, J. J. Diaz Leon, D. Sacchetto, G. Cattaneo, M. Despeisse, M. Boccard, S. Nicolay, Q. Jeangros, B. Niesen, C. Ballif, *Nat. Mater.* **2018**, *17*, 820.
[103] K. A. Bush, A. F. Palmstrom, Z. J. Yu, M. Boccard, R. Cheacharoen, J. P. Mailoa, D. P. McMeekin, R. L. Z. Hoye, C. D. Bailie, T. Leijtens, I. M. Peters, M. C. Minichetti, N. Rolston, R. Prasanna, S. Sofia, D. Harwood, W. Ma, F. Moghadam, H. J. Snaith, T. Buonassisi, Z. C. Holman, S. F. Bent, M. D. McGehee, *Nat. Energy* **2017**, *2*, 17009.
[104] C. Zhang, M. Chen, F. Fu, H. Zhu, T. Feurer, W. Tian, C. Zhu, K. Zhou, S. Jin, S. M. Zakeeruddin, A. N. Tiwari, N. P. Padture, M. Grätzel, Y. Shi, *Energy Environ. Sci.* **2022**, *15*, 1536.
[105] A. Al-Ashouri, E. Kohnen, B. Li, A. Magomedov, H. Hempel, P. Caprioglio, J. A. Marquez, A. B. Morales Vilches, E. Kasparavicius, J. A. Smith, N. Phung, D. Menzel, M. Grischek, L. Kegelmann, D. Skroblin, C. Gollwitzer, T. Malinauskas, M. Jost, G. Matic, B. Rech, R. Schlatmann, M. Topic, L. Korte, A. Abate, B. Stannowski, D. Neher, M. Stolterfoht, T. Unold, V. Getautis, S. Albrecht, *Science* **2020**, *370*, 1300.
[106] M. B. Upama, M. Wright, N. K. Elumalai, M. A. Mahmud, D. Wang, C. Xu, A. Uddin, *ACS Photonics* **2017**, *4*, 2327.
[107] Y. Dou, Z. Liu, Z. Wu, Y. Liu, J. Li, C. Leng, D. Fang, G. Liang, J. Xiao, W. Li, X. Wei, F. Huang, Y.-B. Cheng, J. Zhong, *Nano Energy* **2020**, *71*, 104567.
[108] K.-S. Chen, J.-F. Salinas, H.-L. Yip, L. Huo, J. Hou, A. K. Y. Jen, *Energy Environ. Sci.* **2012**, *5*, 9551.
[109] L. Kranz, A. Abate, T. Feurer, F. Fu, E. Avancini, J. Lockinger, P. Reinhard, S. M. Zakeeruddin, M. Gratzel, S. Buecheler, A. N. Tiwari, *J. Phys. Chem. Lett.* **2015**, *6*, 2676.
[110] Y. Hou, X. Du, S. Scheiner, D. P. McMeekin, Z. Wang, N. Li, M. S. Killian, H. Chen, M. Richter, I. Levchuk, N. Schrenker, E. Spiecker, T. Stubhan, N. A. Luechinger, A. Hirsch, P. Schmuki, H. P. Steinruck,

© 2022 Wiley-VCH GmbH

R. H. Fink, M. Halik, H. J. Snaith, C. J. Brabec, *Science* **2017**, *358*, 1192.
[111] F. J. Ramos, S. Jutteau, J. Posada, A. Bercegol, A. Rebai, T. Guillemot, R. Bodeux, N. Schneider, N. Loones, D. Ory, C. Broussillou, G. Goaer, L. Lombez, J. Rousset, *Sci. Rep.* **2018**, *8*, 16139.
[112] H. H. Park, J. Kim, G. Kim, H. Jung, S. Kim, C. S. Moon, S. J. Lee, S. S. Shin, X. Hao, J. S. Yun, M. A. Green, A. W. Y. Ho-Baillie, N. J. Jeon, T.-Y. Yang, J. Seo, *Small Methods* **2020**, *4*, 2000074.
[113] R. A. Jagt, T. N. Huq, S. A. Hill, M. Thway, T. Liu, M. Napari, B. Roose, K. Gałkowski, W. Li, S. F. Lin, S. D. Stranks, J. L. MacManus-Driscoll, R. L. Z. Hoye, *ACS Energy Lett.* **2020**, *5*, 2456.
[114] B. Chen, Y. Bai, Z. Yu, T. Li, X. Zheng, Q. Dong, L. Shen, M. Boccard, A. Gruverman, Z. Holman, J. Huang, *Adv. Energy Mater.* **2016**, *6*, 1601128.
[115] D. Yang, X. Zhang, Y. Hou, K. Wang, T. Ye, J. Yoon, C. Wu, M. Sanghadasa, S. Liu, S. Priya, *Nano Energy* **2021**, *84*, 105934.
[116] Z. Wang, X. Zhu, S. Zuo, M. Chen, C. Zhang, C. Wang, X. Ren, Z. Yang, Z. Liu, X. Xu, Q. Chang, S. Yang, F. Meng, Z. Liu, N. Yuan, J. Ding, S. Liu, D. Yang, *Adv. Funct. Mater.* **2019**, *30*, 1908298.
[117] T. Gahlmann, K. O. Brinkmann, T. Becker, C. Tückmantel, C. Kreusel, F. Hassend, S. Weber, T. Riedl, *Adv. Energy Mater.* **2020**, *10*, 1903897.
[118] A. Moeini, L. Martinez-Sarti, K. P. S. Zanoni, M. Sessolo, D. Tordera, H. J. Bolink, *J. Mater. Chem. C* **2022**, *10*, 13878.
[119] G. Lin, Y. Lin, B. Sun, *Nanotechnology* **2022**, *33*, 085204.
[120] Y. Wang, T. Mahmoudi, H.-Y. Yang, K. S. Bhat, J.-Y. Yoo, Y.-B. Hahn, *Nano Energy* **2018**, *49*, 59.
[121] B.-X. Chen, H.-S. Rao, H.-Y. Chen, W.-G. Li, D.-B. Kuang, C.-Y. Su, *J. Mater. Chem. A* **2016**, *4*, 15662.
[122] H.-C. Kwon, A. Kim, H. Lee, D. Lee, S. Jeong, J. Moon, *Adv. Energy Mater.* **2016**, *6*, 1601055.
[123] W. Chen, J. Zhang, G. Xu, R. Xue, Y. Li, Y. Zhou, J. Hou, Y. Li, *Adv. Mater.* **2018**, *30*, 1800855.
[124] E. Smecca, V. Valenzano, S. Valastro, I. Deretzis, G. Mannino, G. Malandrino, G. Accorsi, S. Colella, A. Rizzo, A. L. Magna, A. Listorti, A. Alberti, *J. Mater. Chem. A* **2021**, *9*, 16456.
[125] M. Wang, F. Cao, M. Wang, K. Deng, L. Li, *Adv. Mater.* **2021**, *33*, 2006745.
[126] Y. Yang, C. Liu, H. Kanda, Y. Ding, H. Huang, H. Chen, B. Ding, Y. Liang, X. L., M. Cai, P. J. Dyson, S. Dai, M. K. Nazeeruddin, *Adv. Funct. Mater.* **2021**, *31*, 2104868.
[127] Y. Yanagisawa, Y. Nan, K. Okuro, T. Aida, *Science* **2018**, *359*, 72.
[128] W. Urban, D. Davydovich, Y. Yang, T. Demir, Y. Zhang, L. Casabianca, *Science* **2018**, *362*, 220.
[129] J. Lai, J. Mei, X. Jia, C. Li, X. You, Z. Bao, *Adv. Mater.* **2016**, *28*, 8277.
[130] Y. Zhao, J. Wei, H. Li, Y. Yan, W. Zhou, D. Yu, Q. Zhao, *Nat. Commun.* **2016**, *7*, 10228.
[131] H. Zhang, J. Shi, L. Zhu, Y. Luo, D. Li, H. Wu, Q. Meng, *Nano Energy* **2018**, *43*, 383.
[132] Y. Niu, D. He, Z. Zhang, J. Zhu, T. Gavin, P. Falaras, L. Hu, *J. Energy Chem.* **2022**, *68*, 12.
[133] J. Fan, Y. Ma, C. Zhang, C. Liu, W. Li, R. E. I. Schropp, Y. Mai, *Adv. Energy Mater.* **2018**, *8*, 1703421.
[134] X. Meng, Z. Xing, X. Hu, Z. Huang, T. Hu, L. Tan, F. Li, Y. Chen, *Angew. Chem., Int. Ed.* **2020**, *59*, 16602.
[135] M. Wang, H. Sun, F. Cao, W. Tian, L. Li, *Adv. Mater.* **2021**, *33*, 2100625.
[136] K. Zhang, Y. Deng, X. Shi, X. Li, D. Qi, B. Jiang, Y. Huang, *Angew. Chem., Int. Ed.* **2022**, *61*, 202112673.
[137] C. Ge, X. Liu, Z. Yang, H. Li, W. Niu, X. Liu, Q. Dong, *Angew. Chem., Int. Ed.* **2022**, *61*, 202116602.
[138] E. Hoke, D. Slotcavage, E. Dohner, A. Bowring, H. Karunadasa, M. McGehee, *Chem. Sci.* **2015**, *6*, 613.
[139] W. Nie, J. C. Blancon, A. J. Neukirch, K. Appavoo, H. Tsai, M. Chhowalla, M. A. Alam, M. Y. Sfeir, C. Katan, J. Even, S. Tretiak, J. J. Crochet, G. Gupta, A. D. Mohite, *Nat. Commun.* **2016**, *7*, 11574.
[140] F. Lang, N. H. Nickel, J. Bundesmann, S. Seidel, A. Denker, S. Albrecht, V. V. Brus, J. Rappich, B. Rech, G. Landi, H. C. Neitzert, *Adv. Mater.* **2016**, *28*, 8726.
[141] M. B. Al-Handawi, G. Dushaq, P. Commins, D. P. Karothu, M. Rasras, L. Catalano, P. Naumov, *Adv. Mater.* **2022**, *34*, 2109374.
[142] Z. Lou, G. Shen, *Small Struct.* **2021**, *2*, 2000152.
[143] C.-K. Liu, H.-L. Loi, J. Cao, G. Tang, F. Liu, Q. Huang, X. Liang, F. Yan, *Small Struct.* **2021**, *2*, 2000084.
[144] J. Kim, S. Song, Y.-H. Kim, S. K. Park, *Small Struct.* **2021**, *2*, 2000024.



Wei Tian received his Ph.D. degree from Waseda University, Japan, in 2014. Afterward, he joined the National Institute for Materials Science (NIMS), Japan, as a postdoctoral researcher. Currently, he is a professor at Soochow University, China. His research interests include the controlled fabrication and characterization of low-dimensional semiconducting nanostructures and their application in optoelectronics devices.

© 2022 Wiley-VCH GmbH



Liang Li received his Ph.D. degree from the Institute of Solid State Physics, Chinese Academy of Sciences in 2006. From 2007–2012, he worked at the National University of Singapore (NUS), Singapore, the National Institute of Advanced Industrial Science and Technology (AIST), Japan, the National Institute of Materials Science (NIMS), Japan, and the University of Western Ontario (UWO), Canada. Since August 2012, he is a full professor at Soochow University, China. His research group focuses mainly on energy conversion materials for solar cells, photodetectors, and electrochemical batteries.

© 2022 Wiley-VCH GmbH